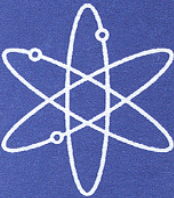




Parametric Study of the Effect of Control Rods for PWR Burnup Credit



Prepared by
C. E. Sanders and J. C. Wagner, ORNL



Oak Ridge National Laboratory



U.S. Nuclear Regulatory Commission
Office of Nuclear Regulatory Research
Washington, DC 20555-0001



AVAILABILITY OF REFERENCE MATERIALS IN NRC PUBLICATIONS

NRC Reference Material

As of November 1999, you may electronically access NUREG-series publications and other NRC records at NRC's Public Electronic Reading Room at www.nrc.gov/NRC/ADAMS/index.html.

Publicly released records include, to name a few, NUREG-series publications; *Federal Register* notices; applicant, licensee, and vendor documents and correspondence; NRC correspondence and internal memoranda; bulletins and information notices; inspection and investigative reports; licensee event reports; and Commission papers and their attachments.

NRC publications in the NUREG series, NRC regulations, and *Title 10, Energy*, of the Code of *Federal Regulations*, may also be purchased from one of these two sources:

1. The Superintendent of Documents
U.S. Government Printing Office
P.O. Box 37082
Washington, DC 20402-9328
www.access.gpo.gov/su_docs
202-512-1800
2. The National Technical Information Service
Springfield, VA 22161-0002
www.ntis.gov
1-800-553-6847 or, locally, 703-605-6000

A single copy of each NRC draft report for comment is available free, to the extent of supply, upon written request as follows:

Address: Office of the Chief Information Officer,
Reproduction and Distribution
Services Section
U.S. Nuclear Regulatory Commission
Washington, DC 20555-0001

E-mail: DISTRIBUTION@nrc.gov

Facsimile: 301-415-2289

Some publications in the NUREG series that are posted at NRC's Web site address www.nrc.gov/NRC/NUREGS/indexnum.html are updated regularly and may differ from the last printed version.

Non-NRC Reference Material

Documents available from public and special technical libraries include all open literature items, such as books, journal articles, and transactions, *Federal Register* notices, Federal and State legislation, and congressional reports. Such documents as theses, dissertations, foreign reports and translations, and non-NRC conference proceedings may be purchased from their sponsoring organization.

Copies of industry codes and standards used in a substantive manner in the NRC regulatory process are maintained at—

The NRC Technical Library
Two White Flint North
11545 Rockville Pike
Rockville, MD 20852-2738

These standards are available in the library for reference use by the public. Codes and standards are usually copyrighted and may be purchased from the originating organization or, if they are American National Standards, from—

American National Standards Institute
11 West 42nd Street
New York, NY 10036-8002
www.ansi.org
212-642-4900

The NUREG series comprises (1) technical and administrative reports and books prepared by the staff (NUREG/XXXX) or agency contractors (NUREG/CR-XXXX), (2) proceedings of conferences (NUREG/CP-XXXX), (3) reports resulting from international agreements (NUREG/IA-XXXX), (4) brochures (NUREG/BR-XXXX), and (5) compilations of legal decisions and orders of the Commission and Atomic and Safety Licensing Boards and of Directors' decisions under Section 2.206 of NRC's regulations (NUREG-0750).

DISCLAIMER: This report was prepared as an account of work sponsored by an agency of the U.S. Government. Neither the U.S. Government nor any agency thereof, nor any employee, makes any warranty, expressed or implied, or assumes any legal liability or responsibility for any third party's use, or the results of such use, of any information, apparatus, product, or process disclosed in this publication, or represents that its use by such third party would not infringe privately owned rights.

Parametric Study of the Effect of Control Rods for PWR Burnup Credit

Manuscript Completed: October 2001
Date Published: February 2002

Prepared by
C. E. Sanders and J. C. Wagner, ORNL

Oak Ridge National Laboratory
Managed by UT-Battelle, LLC
Oak Ridge, TN 37831-6370

R. Y. Lee, NRC Project Manager

Prepared for
Division of System Analysis and Regulatory Effectiveness
Office of Nuclear Regulatory Research
U.S. Nuclear Regulatory Commission
Washington, DC 20555-0001
NRC Job Code W6479



ABSTRACT

The Interim Staff Guidance on burnup credit for pressurized water reactor (PWR) spent nuclear fuel (SNF), issued by the United States Nuclear Regulatory Commission's (U.S. NRC) Spent Fuel Project Office, recommends the use of analyses that provide an "*adequate representation of the physics*" and notes particular concern with the "*need to consider the more reactive actinide compositions of fuels burned with fixed absorbers or with control rods fully or partly inserted.*" In the absence of readily available information on the extent of control rod (CR) usage in U.S. PWRs and the subsequent reactivity effect of CR exposure on discharged SNF, NRC staff has indicated a need for greater understanding in these areas. In response, this report presents a parametric study of the effect of CR exposure on the reactivity of discharged SNF for various CR designs, including Axial Power Shaping Rods, fuel enrichments, and exposure conditions (i.e., burnup and axial insertion). The study is performed in two parts. In the first part, two-dimensional assembly calculations are performed, effectively assuming full axial CR insertion. These calculations bound the effect of CR exposure and facilitate comparisons of the various CR designs. In the second part, three-dimensional calculations are performed to quantify the reactivity effect of CR exposure in a burnup credit cask environment and determine the effect of partly inserted CRs. The reactivity effect as a function of axial insertion depth is shown for the various CR designs considered. The results from the study demonstrate that the reactivity effect increases with increasing CR exposure (e.g., burnup) and decreasing initial fuel enrichment (for a fixed burnup). Further, CR exposure is shown to have a larger effect on discharge reactivity when it occurs later in the assembly burnup. For variations in CR design, there exists a direct relationship between the reactivity worth of the CRs and their effect on discharge reactivity – higher reactivity worth CRs result in larger effects on discharge reactivity. The effects are quantified and typical operating conditions are reviewed, enabling an increased understanding of the effect of CR exposure on the reactivity of discharged SNF. The report concludes with a discussion of the issues for consideration and preliminary recommendations to address the effect of CR exposure in burnup credit criticality safety analyses.

CONTENTS

	<u>Page</u>
ABSTRACT.....	iii
LIST OF FIGURES.....	vii
LIST OF TABLES.....	ix
FOREWORD.....	xi
ACKNOWLEDGEMENTS.....	xiii
1 INTRODUCTION.....	1
2 REVIEW OF CONTROL ROD DESIGNS AND OPERATIONAL PRACTICES.....	3
2.1 CONTROL ROD DESIGNS.....	3
2.1.1 Westinghouse Designs.....	3
2.1.2 Babcock & Wilcox Designs.....	3
2.1.3 Combustion Engineering Designs.....	3
2.2 CONTROL ROD DESIGNS INVESTIGATED.....	3
2.2.1 Hybrid Ag-In-Cd/B ₄ C Control Rod Design (Westinghouse 17 × 17).....	4
2.2.2 Ag-In-Cd Control Rod Design (B&W 15 × 15).....	4
2.2.3 CE Ag-In-Cd/B ₄ C Control Rod Design (CE 14 × 14).....	4
2.2.4 Axial Power Shaping Rod Design (B&W 15 × 15).....	4
2.3 CONTROL RODS OPERATIONAL PRACTICES.....	4
3 REACTIVITY EFFECT OF CONTROL RODS.....	7
3.1 INTRODUCTION AND BACKGROUND.....	7
3.2 TWO-DIMENSIONAL ANALYSES.....	7
3.2.1 Code Description.....	7
3.2.2 Calculations.....	8
3.2.3 B&W Ag-In-Cd Control Rods.....	9
3.2.4 Westinghouse Hybrid Ag-In-Cd/B ₄ C Control Rods.....	17
3.2.5 CE Ag-In-Cd/B ₄ C Control Rods.....	24
3.2.6 B&W Gray Axial Power Shaping Rods.....	29
3.2.7 Cooling Time.....	35
3.2.8 Summary of Two-Dimensional Analyses.....	36
3.3 THREE-DIMENSIONAL ANALYSES.....	38
3.3.1 Code Description.....	39
3.3.2 Reactivity Behavior with CRs Present for a Rail-Type Cask.....	39
3.3.2.1 Full-Axial Insertion Analyses.....	41
3.3.2.2 Partial-Axial Insertion Analyses.....	46
4 DISCUSSION AND IMPLICATIONS.....	51
5 RECOMMENDATIONS.....	53
6 REFERENCES.....	55

LIST OF FIGURES

<u>Figure</u>	<u>Page</u>
1 B&W 15 × 15 assembly lattice representing the CR locations.....	10
2 HELIOS calculational model of a B&W 15 × 15 assembly containing 16 CRs	11
3 Comparison of k_{inf} values (out-of-reactor conditions) as a function of burnup. The results correspond to 4 wt % ^{235}U enriched B&W 15 × 15 fuel and Ag-In-Cd CRs.....	12
4 Comparison of Δk values as a function of burnup for various CR exposures with initial fuel enrichments of 3, 4, and 5 wt % ^{235}U , for B&W 15 × 15 fuel and Ag-In-Cd CRs.....	14
5 Comparison of Δk values as a function of burnup for 5 GWd/MTU CR exposures at various times during the burnup with 4 wt % ^{235}U B&W 15 × 15 fuel and Ag-In-Cd CRs.....	15
6 Comparison of Δk values as a function of burnup with CR exposure during the first 15 GWd/MTU (1 cycle) for various initial fuel enrichments. The results correspond to B&W 15 × 15 fuel and Ag-In-Cd CRs.....	16
7 Westinghouse 17 × 17 assembly lattice representing the CR locations	18
8 HELIOS calculational model of a Westinghouse 17 × 17 assembly containing 24 CRs	19
9 Comparison of k_{inf} values (out-of-reactor conditions) as a function of burnup with and without CR exposure. The results correspond to 4 wt % ^{235}U enriched Westinghouse 17 × 17 fuel and Ag-In-Cd/B ₄ C CRs.	20
10 Comparison of Δk values as a function of burnup for various CR exposures with initial fuel enrichments of 3, 4, and 5 wt % ^{235}U . The results correspond to Westinghouse 17 × 17 fuel and the B ₄ C axial segment of the hybrid Ag-In-Cd/B ₄ C CRs.	22
11 Comparison of Δk values as a function of burnup for 5 GWd/MTU CR exposures at various times during the burnup with initial fuel enrichment of 4 wt % ^{235}U . The results correspond to Westinghouse 17 × 17 fuel and B ₄ C CRs.....	23
12 CE 14 × 14 assembly lattice representing the CR locations	25
13 HELIOS calculational model of a CE 14 × 14 assembly containing five CRs	26
14 Comparison of k_{inf} (out-of-reactor conditions) as a function of burnup with and without CR exposure. The results correspond to 4 wt % ^{235}U enriched CE 14 × 14 fuel and the B ₄ C axial segment of the Ag-In-Cd/B ₄ C CRs.	27
15 Comparison of Δk values as a function of burnup for various CR exposures with initial fuel enrichments of 3, 4, and 5 wt % ^{235}U . The results correspond to CE 14 × 14 fuel and the B ₄ C axial segment of the Ag-In-Cd/B ₄ C CRs.	28
16 B&W 15 × 15 assembly lattice representing the APSR locations.....	31

LIST OF FIGURES (continued)

<u>Figure</u>	<u>Page</u>
17	Comparison of k_{inf} values (out-of-reactor conditions) as a function of burnup with and without APSR exposure. The results correspond to 4 wt % ^{235}U enriched B&W 15×15 fuel and gray APSRs.32
18	Comparison of Δk values as a function for various APSR exposures with initial fuel enrichments of 3, 4, and 5 wt % ^{235}U . The results correspond to B&W 15×15 fuel and gray APSRs.33
19	Comparison of Δk values as a function of burnup with APSR exposure during the first 30 GWd/MTU (2 cycles) for various initial fuel enrichments. The results correspond to B&W 15×15 fuel and gray APSRs.....34
20	Comparison of Δk values as a function of burnup for 15 GWd/MTU APSR exposures at various times during the burnup with initial fuel enrichment of 4 wt % ^{235}U . The results correspond to B&W 15×15 fuel and gray APSRs.35
21	Comparison of Δk values as a function of burnup for various cooling times for 45 GWd/MTU CR exposures with initial fuel enrichment of 4 wt % ^{235}U . The results correspond to Westinghouse 17×17 fuel and the B ₄ C segment of the Ag-In-Cd/B ₄ C CRs.....36
22	Comparison of Δk values for an infinite assembly array (45 GWd/MTU, 0-year cooling time) with various CR exposures. The results correspond to fuel with 4.0 wt % ^{235}U initial enrichment.37
23	Relationship between the effect of CR exposure on discharge reactivity (in terms of Δk) and CR initial reactivity worth (in terms of $\Delta k/k$) for each of the CR and APSR designs considered. The results correspond to fuel with 45 GWd/MTU burnup and 4.0 wt % ^{235}U initial enrichment that have experienced different CR exposure durations. CR exposure durations are continuous, beginning at zero burnup and continuing until the specified burnup exposure (e.g., 5 GWd/MTU exposure occurs from 0–5 GWd/MTU.).....38
24	Cross-sectional view of one quarter of the KENO V.a calculational model of the GBC-32 cask loaded with Westinghouse 17×17 assemblies40
25	Illustration of (a) partially inserted control rods and (b) a cross section of the criticality model.47
26	Δk as a function of axial depth of CR insertion for the GBC-32 cask. Results correspond to 4 wt % ^{235}U enriched Westinghouse 17×17 fuel and B ₄ C/Ag-In-Cd CRs.48
27	Δk as a function of axial depth of CR insertion for the GBC-32 cask. Results correspond to 4 wt % ^{235}U enriched B&W 15×15 fuel and Ag-In-Cd CRs.....49
28	Δk as a function of axial depth of CR insertion for the GBC-32. Results correspond to 4 wt % ^{235}U enriched CE 14×14 fuel and B ₄ C CRs.50

LIST OF TABLES

<u>Table</u>	<u>Page</u>
1 Summary of parameters used for the depletion calculations.....	8
2 B&W 15 × 15 fuel assembly and CR specifications	9
3 Summary of maximum positive Δk values observed for B&W Ag-In-Cd CR cases considered	15
4 Westinghouse 17 × 17 fuel assembly and CR specifications	17
5 Summary of maximum positive Δk values observed for B ₄ C axial segment of the Westinghouse hybrid Ag-In-Cd/B ₄ C CR cases considered	23
6 CE 14 × 14 fuel assembly and CR specifications.....	24
7 Summary of maximum positive Δk values observed for the B ₄ C axial segment of the CE Ag-In-Cd/B ₄ C CR cases considered.....	29
8 B&W 15 × 15 fuel assembly and APSR specifications	30
9 Summary of maximum positive Δk values observed for B&W APSR cases considered	34
10 Nuclides associated with the various classifications of burnup credit	41
11 Value of k_{eff} for various CR exposures for actinide-only burnup credit in the GBC-32 cask. Results correspond to Westinghouse 17 × 17 fuel with 4 wt % ²³⁵ U enrichment and B ₄ C CRs fully inserted during depletion.....	42
12 Value of k_{eff} for various CR exposures for actinide + fission product burnup credit in the GBC-32 cask. Results correspond to Westinghouse 17 × 17 fuel with 4 wt % ²³⁵ U enrichment and B ₄ C CRs fully inserted during depletion.....	42
13 Value of k_{eff} for various CR exposures for actinide-only burnup credit in the GBC-32 cask. Results correspond to Westinghouse 17 × 17 fuel with 4 wt % ²³⁵ U enrichment and B ₄ C (top part, approximately 160 cm)/ Ag-In-Cd (lower part, approximately 102 cm) CRs fully inserted during depletion	43
14 Value of k_{eff} for various CR exposures for actinide + fission product burnup credit in the GBC-32 cask. Results correspond to Westinghouse 17 × 17 fuel with 4 wt % ²³⁵ U enrichment and B ₄ C (top part, approximately 160 cm)/ Ag-In-Cd (lower part, approximately 102 cm) CRs fully inserted during depletion	43
15 Value of k_{eff} for various CR exposures for actinide-only burnup credit in the GBC-32 cask. Results correspond to B&W 15 × 15 fuel with 4 wt % ²³⁵ U enrichment and Ag-In-Cd CRs fully inserted during depletion.....	44

LIST OF TABLES (continued)

<u>Table</u>		<u>Page</u>
16	Value of k_{eff} for various CR exposures for actinide + fission product burnup credit in the GBC-32 cask. Results correspond to B&W 15×15 fuel with 4 wt % ^{235}U enrichment and Ag-In-Cd CRs fully inserted during depletion.....	44
17	Value of k_{eff} for various CR exposures for actinide-only burnup credit in the GBC-32 cask. Results correspond to CE 14×14 fuel with 4 wt % ^{235}U enrichment and B ₄ C CRs fully inserted during depletion.	45
18	Value of k_{eff} for various CR exposures for actinide + fission product burnup credit in the GBC-32 cask. Results correspond to CE 14×14 fuel with 4 wt % ^{235}U enrichment and B ₄ C CRs fully inserted during depletion	45

FOREWORD

In 1999 the United States Nuclear Regulatory Commission (NRC) issued initial recommended guidance for using reactivity credit due to fuel irradiation (i.e., burnup credit) in the criticality safety analysis of spent pressurized-water-reactor (PWR) fuel in storage and transportation packages. This guidance was issued by the NRC Spent Fuel Project Office (SFPO) as Revision 1 to Interim Staff Guidance 8 (ISG8R1) and published in the *Standard Review Plan for Transportation Packages for Spent Nuclear Fuel*, NUREG-1617 (March 2000). With this initial guidance as a basis, the NRC Office of Nuclear Regulatory Research initiated a program to provide the SFPO with technical information that would:

- enable realistic estimates of the subcritical margin for systems with spent nuclear fuel (SNF) and an increased understanding of the phenomena and parameters that impact the margin, and
- support the development of technical bases and recommendations for effective implementation of burnup credit and provide realistic SNF acceptance criteria while maintaining an adequate margin of safety.

The ISG8R1 recommends that consideration be given to the increased reactivity of SNF resulting from the presence of control rods (CRs) in the fuel during a portion of the irradiation. This report presents a parametric study that quantifies the changes in the SNF neutron multiplication factor as a function of the CR insertion (axial depth into fuel as well as burnup duration) and discusses the behavior that causes the changes. The results provide a basis for efficiently and effectively estimating the impact of CR exposure within typical domestic PWR operations (CRs resting at the top of the fuel and full-axial insertions of short burnup duration).



Farouk Eltawila, Director
Division of Systems Analysis and Regulatory Effectiveness

ACKNOWLEDGEMENTS

This work was supported by the Office of Nuclear Regulatory Research, Nuclear Regulatory Commission under Project JCN W6479, Development and Applicability of Criticality Safety Software for Licensing Review. The authors acknowledge review and useful comments by Carl J. Withee of the Spent Fuel Project Office.

The thorough review of the manuscript by our colleagues R. M. Westfall, S. M. Bowman, M. D. DeHart, J. C. Gehin, R. T. Primm, and C. V. Parks is much appreciated. Also, the authors are grateful to W. C. Carter and J. B. Anderson for their careful preparation of this report. In addition, thanks to S. K. Lichtenwalter for her consultation.

1 INTRODUCTION

The concept of taking credit for the reduction in reactivity due to the fuel burnup is commonly referred to as burnup credit. The reduction in reactivity that occurs with fuel burnup is due to the change in concentration (net reduction) of fissile nuclides and the production of actinide and fission-product neutron absorbers. The change in the concentration of these nuclides with fuel burnup, and consequently the reduction in reactivity, is dependent upon the depletion environment (e.g., the neutron spectrum). In contrast to criticality safety analyses that employ the “fresh-fuel assumption,” the utilization of credit for fuel burnup therefore necessitates consideration of all possible fuel operating conditions, including exposure to control rods (CRs).

The Interim Staff Guidance¹ on burnup credit (ISG-8) for pressurized water reactor (PWR) spent nuclear fuel (SNF), issued by the United States Nuclear Regulatory Commission’s (U.S. NRC) Spent Fuel Project Office, recommends the use of analyses that provide an “adequate representation of the physics” and notes particular concern with the “need to consider the more reactive actinide compositions of fuels burned with fixed absorbers or with control rods fully or partly inserted.” In the absence of readily available information on the extent of CR usage in U.S. PWRs and the subsequent reactivity effect of CR exposure on discharged SNF, NRC staff has indicated² a need for greater understanding in these areas. In response, this report presents a parametric study of the effect of CR exposure on the reactivity of discharged SNF for various CR designs, including axial power shaping rods (APSRs), fuel enrichments, and exposure conditions (i.e., burnup and axial insertion). Herein, APSRs are included in the general classification of CRs, but are discussed separately where differences exist (e.g., usage/operations). The effects of fixed absorbers, such as burnable poison rods (BPRs) and integral burnable absorbers (IBAs), on the reactivity of SNF are addressed elsewhere.^{3,4}

The presence of CRs/APSRs increases the reactivity of burned fuel by hardening the neutron spectrum (due to removal of thermal neutrons by capture and displacement of moderator) and suppressing burnup in localized regions. The former effect results in an increased production of fissile plutonium isotopes and a decrease in ²³⁵U fission, while the latter effect can lead to axial burnup distributions characterized by significantly under-burned regions. Consequently, an assembly exposed to CRs can have a higher reactivity for a given burnup than an assembly that has not been exposed to CRs. Although the axial burnup distribution is an important concern for burnup credit evaluations, the effect of CR/APSR insertion on the axial burnup distribution is not addressed here because it is considered in the selection of bounding axial burnup profile(s).^{5,6} Instead, this study examines the effect of CR/APSR insertion on reactivity due to the impact of spectral hardening on the spent-fuel isotopics.

Currently in the United States, PWRs operate with the CRs withdrawn or nearly withdrawn and use soluble boron to control the change in reactivity with burnup. In contrast, French PWR operations involve long periods of CR insertion for reactor control, low-power operations and load following.⁷ Similarly, some early domestic operations included notable CR insertions (usually in conjunction with an assembly’s first cycle of burnup).⁸ Axial power shaping rods, on the other hand, are inserted during “normal” reactor operation, but are relatively few in number (e.g., in the Three Mile Island Unit-1 reactor, eight assemblies/core may contain APSRs, while 24 assemblies/core may contain CRs⁹). Fuel shuffling between cycles reduces the probability that a fuel assembly will be exposed to CR/APSR insertions for more than one cycle.

Because of the variability in CR and APSR usage, estimating the effect of CRs and APSRs in a generic manner is difficult. Therefore parametric analyses were performed for a variety of exposure scenarios to establish an increased understanding of the effect of CR exposure on the reactivity of discharged SNF. Effects are quantified and typical operating conditions are reviewed. Although many of the scenarios considered are not representative of actual reactor operations, it should be possible to estimate the reactivity effect of specific CR exposure conditions based on inspection of the calculated results and trends shown in this report.

The study described in this report is performed in two parts. In the first part, two-dimensional (2-D) calculations are performed, effectively assuming full axial CR exposure (i.e., fully inserted). These calculations are intended to bound the effect of CR exposure and facilitate comparisons of the various CR designs. Several CR designs (including APSRs) that have been widely used in U.S. commercial PWRs are included in this study. In the second part, three-dimensional (3-D) calculations are performed to quantify the reactivity effect in a burnup credit cask environment and to determine the effect of partly inserted CRs and gain a better understanding of reality. The reactivity effect as a function of axial insertion depth is shown for the various CR designs considered. Note that the effect of the CRs is determined based on their effect on the depletion isotopics alone (i.e., the CRs are not included in the criticality models, since these models represent out-of-reactor conditions).

2 REVIEW OF CONTROL ROD DESIGNS AND OPERATIONAL PRACTICES

2.1 CONTROL ROD DESIGNS

Several different CR designs have been used in commercial nuclear reactors. However, all CR designs are similar in that they contain thermal neutron absorbing material in rods sized to fit within the assembly guide tubes. The Westinghouse, Combustion Engineering (CE), and Babcock & Wilcox (B&W) CR designs, including B&W APSRs, were considered in this report. Note that B&W is the only U.S. PWR fuel vendor known to use APSRs.

2.1.1 Westinghouse Designs

Westinghouse has manufactured various types of CRs for 14×14 , 15×15 , and 17×17 fuel lattices.¹⁰ Full- and part-length silver-indium-cadmium (Ag-In-Cd) CRs with stainless steel cladding have been manufactured for the 16 CR locations in the 14×14 fuel assembly designs. For the 20 CR locations in the 15×15 fuel assembly designs, full-length Ag-In-Cd CRs with stainless steel cladding are used. For the 24 CR locations in the 17×17 fuel assembly designs, the following four different CR designs, all with stainless steel cladding, have been used: (1) full-length “hybrid” CRs, using 102 in. (~259 cm) of boron carbide (B_4C) and 40 in. (~102 cm) of Ag-In-Cd, (2) full-length Ag-In-Cd CRs, (3) full-length hafnium (Hf) CRs (many reactors have been replacing these with Ag-In-Cd rods because of irradiation induced swelling), and (4) part-length CRs, using 36 in. (~91 cm) of Ag-In-Cd with a 106 in. (~269 cm) aluminum oxide spacer.

2.1.2 Babcock & Wilcox Designs

Babcock & Wilcox has manufactured two main types of CRs for 15×15 fuel assembly designs with 16 CR locations: (1) Ag-In-Cd CRs with stainless steel cladding and (2) gray/black APSRs with stainless steel cladding. The APSRs consist of either part-length Ag-In-Cd absorber (black APSRs) or Inconel absorber (gray APSRs).¹¹ The absorber region in the black APSRs is 36 in. (~91 cm) tall while the absorber region in the gray APSRs is 63 in. (~160 cm) tall.

2.1.3 Combustion Engineering Designs

Combustion Engineering has manufactured a variety of CR assemblies, referred to as control element assemblies (CEAs), for use in the five CR locations present in their 14×14 and 16×16 fuel assembly designs.^{10,12} For the 14×14 fuel assembly designs, the following different CEAs with Inconel cladding have been used: (1) full-length CEAs with B_4C in the central rod and axial regions of Inconel, Ag-In-Cd, and B_4C in the remaining four rods, (2) part-length CEAs with one B_4C rod and four stainless steel rods, (3) part-length CEAs with one rod of Al_2O_3 and four rods of Ag-In-Cd and B_4C , and (3) part-length CEAs with one rod of Al_2O_3 , two rods of Ag-In-Cd and B_4C , and two rods with stainless steel and Al_2O_3 . Similar variations of full- and part-length CEAs have been manufactured for the 16×16 fuel assembly design.

2.2 CONTROL ROD DESIGNS INVESTIGATED

As evident from the preceding discussion, the variation in CR designs is significant. However, the variation in CR absorber materials is more limited, namely B_4C , Ag-In-Cd, Hf, and Inconel. Rather than attempt to

investigate each of the numerous CR designs, which in many cases involve relatively minor differences, analyses in this report focused on investigating unique CR designs and materials to establish greater understanding. The effects of CR designs that use the same absorber material are expected to be similar. The CR designs analyzed in this report are the (1) Westinghouse 17×17 hybrid Ag-In-Cd/B₄C CR design, (2) B&W 15×15 Ag-In-Cd CR design, (3) CE 14×14 B₄C CR design, and (4) B&W 15×15 gray APSR design. Additional information about the specific CR designs analyzed in this report is provided in the following subsections. Detailed specifications are given in the respective analysis sections.

2.2.1 Hybrid Ag-In-Cd/B₄C Control Rod Design (Westinghouse 17×17)

The hybrid Ag-In-Cd/B₄C rod cluster control assembly (RCCA) developed by Westinghouse and analyzed in this report, consists of B₄C pellets and Ag-In-Cd cylinders encapsulated in stainless steel cladding. Inside each RCCA, the B₄C absorber pellets are stacked on top of the Ag-In-Cd absorber. The total length of the absorber column is 142 in. (~361 cm), where B₄C constitutes 102 in. (~259 cm) and the Ag-In-Cd constitutes 40 in. (~102 cm). The absorber column is sitting on an Inconel coil spring (in the lower part of the absorber rod). The hold-down spring is designed to restrain the absorber material against longitudinal movement during transport, handling, and operation while allowing for differential expansion between the absorber and the clad.¹³

2.2.2 Ag-In-Cd Control Rod Design (B&W 15×15)

The Ag-In-Cd RCCA developed by B&W and analyzed in this report, consists of Ag-In-Cd cylinders encapsulated in stainless steel cladding. The 134-in. long absorber column sits on a lower-end plug made of stainless steel. The upper end plug (also known as the spring spacer) is also made of stainless steel and designed to restrain the absorber material against longitudinal movement during transport, handling, and operation.¹¹

2.2.3 CE Ag-In-Cd/B₄C Control Rod Design (CE 14×14)

The CEA developed by CE and analyzed in this report, consists of five Inconel tubes (fingers) that are stacked with cylindrical B₄C pellets.¹² The lower 8 in. (~20 cm) of the fingers are filled with Ag-In-Cd material. The CEAs are 161 in. (~409 cm) long, with 134 in. (~340 cm) and 124 in. (~315 cm) of B₄C in the center and outer fingers, respectively. A plenum is positioned above the poison pellet column to allow expansion volume. The plenum also contains a spring that prevents the absorber material from moving during shipping and handling. Each finger is sealed with an Inconel cap at the bottom and an Inconel end fitting at the top.¹²

2.2.4 Axial Power Shaping Rod Design (B&W 15×15)

The APSRs developed by B&W consist of part-length absorber rods encapsulated in stainless steel cladding. As mentioned, the APSRs can either be gray (Inconel) or black (Ag-In-Cd). The gray APSRs are only considered in this report due to the fact that the black APSRs are very similar to the Ag-In-Cd CR that is analyzed in this report.

2.3 CONTROL RODS OPERATIONAL PRACTICES

Because the effect of CRs on reactivity is dependent on the duration and extent (i.e., axial insertion) of CR exposure and the fraction of burnup without CRs inserted, it is important to understand typical operational practices. However, because of operational variability, the extent of CR usage varies, making it difficult to truly

characterize “typical” operational practice. With this in mind, some general observations related to “typical” CR operational practices are given in this section.

During full-power operation CRs are typically inserted into the upper portion of the fuel assemblies – above the active fuel region. It is fairly common for the CRs to be inserted about 20 cm for the majority of the entire burnup cycle.^{7, 14-16} This insertion depth is above the active fuel region, so the fuel is not exposed to the CRs. When inserted into the active fuel region, CRs are either inserted into a small region of the upper portion of the active fuel or fully inserted during reactor shutdown. Note, however, that some early domestic operations included notable CR insertions (usually in conjunction with an assembly’s first cycle of burnup).⁸

Axial power shaping rods are utilized in the active fuel region during “normal” reactor operation. The APSRs are typically inserted into fuel assemblies that have been previously irradiated (second or third cycle).^{9,11} The APSRs remain partially inserted until the end (or near the end) of the burnup cycle.

3 REACTIVITY EFFECT OF CONTROL RODS

3.1 INTRODUCTION AND BACKGROUND

Since the presence of the CRs hardens the spectrum during depletion, the production of fissile plutonium increases while the depletion of ^{235}U decreases. This occurrence increases the reactivity of the fuel at discharge and beyond. Hence, an assembly exposed to CRs can have a higher reactivity for a given burnup than an assembly that has not been exposed to CRs.

Due to the great variability in CR and APSR usage, as mentioned earlier, estimating the effect of CRs and APSRs in a generic manner is difficult. Therefore parametric analyses were performed for a variety of exposure scenarios to establish an increased understanding of the effect of CR exposure on the reactivity of discharged SNF. Although many of the scenarios considered are not representative of current U.S. PWR reactor operations, it should be possible to estimate the reactivity effect of actual CR exposure conditions based on inspection of the calculated results and trends.

The study is performed in two parts. In the first part, 2-D calculations are performed with the intent to bound the effect of CR exposure, effectively assuming full axial CR exposure (i.e., fully inserted). In the second part, 3-D calculations are performed to determine the effect of partial CR insertion conditions. Note that the effect of the CRs is determined based on their effect on the depletion isotopics alone (i.e., the CRs are not included in the criticality models).

The following sections describe the calculational methods used for this evaluation and present detailed analyses to demonstrate the reactivity effect of CRs as a function of burnup. The analyses include variations in the type of CR, composition, duration of exposure, axial depth of insertion, and initial fuel assembly enrichment.

3.2 TWO-DIMENSIONAL ANALYSES

3.2.1 Code Description

The 2-D calculations presented in the following subsections were performed using the HELIOS-1.6 code package,¹⁷ which primarily consists of three programs: AURORA, HELIOS, and ZENITH. HELIOS is a 2-D, generalized-geometry transport theory code based on the method of collision probabilities with current coupling. AURORA, the input processor, is used to define the geometry, materials, and calculational parameters. ZENITH, the output processor, reads the results saved by HELIOS (in a binary database) and outputs the results in text format. The HELIOS code system also contains the ORION program for viewing and checking model geometries and materials.

HELIOS was employed for this analysis because of its capability to explicitly model the relatively complicated, heterogeneous assembly lattices associated with CRs. The various structures within each of the assembly models were coupled using angular current discretization (interface currents). All calculations are for an infinite array of fuel assemblies and utilize the 45-group neutron cross-section library, based on ENDF/B-VI, which is distributed with the HELIOS-1.6 code package.

It should be pointed out that since there is a balance between the number of neutrons produced (from fissions) and the number of neutrons lost (either by absorption or leakage) in a critical reactor, concerns have arisen that when performing calculations this balance may not be accurately described and consequently the spectrum in the computational model may not agree with critical reactor conditions. In general, for the systems considered in this

report, the calculated neutron multiplication factor, k , is not equal to unity. However, the systems are assumed to be part of a critical reactor (i.e., $k = 1$). The HELIOS code, by default, compensates for this difference by approximating the criticality spectrum based on an adjustment of the net out-leakage if $k > 1$ or the net in-leakage if $k < 1$. A few calculations were performed with a user specified buckling value to override the use of the HELIOS calculated criticality spectrum and assess the spectral variations and consequent effects on reactivity. The conclusion from these calculations is that, for the purpose of the studies presented in this report, the default criticality spectrum calculated by HELIOS is the most appropriate one to use.

3.2.2 Calculations

All depletion calculations were performed with HELIOS using the properties and parameters given in Table 1. Using the isotopic compositions from the depletion calculations, branch or restart calculations were performed with HELIOS to determine the infinite neutron-multiplication factor, k_{inf} , as a function of burnup for out-of-reactor conditions (i.e., 20° C with no soluble boron present), zero cooling time, and the full nuclide set. Note that all of the 2-D analyses presented in this section include all of the nuclides available in the HELIOS 45-group cross-section library that is distributed as part of the HELIOS-1.6 code package. For each unique CR assembly design considered, a depletion calculation was performed for (1) the uncontrolled assembly condition (i.e., no CRs present) and (2) conditions in which the CRs were assumed to be present for various periods of burnup. Subsequently, separate criticality calculations were performed for out-of-reactor conditions using the isotopic compositions from the depletion calculations. The Δk values between these sets of conditions are reported to assess the effect of CRs on the reactivity of discharge SNF.

The 2-D calculations were done with an infinite radial array of assemblies to gain an understanding of behaviors and trends and so that the results would be general (i.e., not dependent on storage cell specifications, such as poison loading). Three-dimensional results for a specific SNF cask are provided in Section 3.3. A number of the 2-D calculations were repeated in Section 3.2.7 to assess the effect for variations in cooling time. The results demonstrate that the calculated effects are not sensitive to variations in cooling time within the time frame of cask storage and transportation.

Table 1 Summary of parameters used for the depletion calculations

Parameter	Value used in analyses
Moderator temperature (K)	600
Fuel temperature (K)	1000
Fuel density (g/cm ³)	10.44 (UO ₂)
Clad temperature (K)	600
Clad density (g/cm ³)	5.78 (Zr)
Power density* (MW/MTU)	60
Moderator boron concentration (ppm)	650

*Various cases were also calculated using a power density of 30 MW/t (which is a more realistic value). The results showed that the Δk values presented in the following sections are not sensitive to variations in the power density.

3.2.3 B&W Ag-In-Cd Control Rods

The Ag-In-Cd RCCA consists of 16 CRs. Calculations were performed with a B&W 15×15 assembly in order to investigate the reactivity effect of these CRs. Dimensional specifications for the fuel assembly and CRs are given in Table 2 (Ref. 11). The 15×15 B&W assembly lattice considered is shown in Figure 1. Figure 2 displays the geometry of the B&W 15×15 assembly as modeled in HELIOS.

Table 2 B&W 15×15 fuel assembly and CR specifications

Parameter	Dimension (cm)
Fuel assembly specifications	
Rod pitch	1.44272
Assembly pitch	21.81
Cladding outside diameter	1.09220
Cladding inside diameter	0.95758
Pellet outside diameter	0.940
Guide/instrument tube outside diameter	1.34620
Guide/instrument tube inside diameter	1.26492
Array size	15×15
Number of fuel rods	208
Number of guide/instrument tubes	17
Control rod specifications	
Absorber material	Ag (80%)–In (15%)–Cd (5%)
Absorber pellet diameter	0.99568
Cladding (304 SS) outside diameter	1.11760
Cladding (304 SS) inside diameter	1.01092

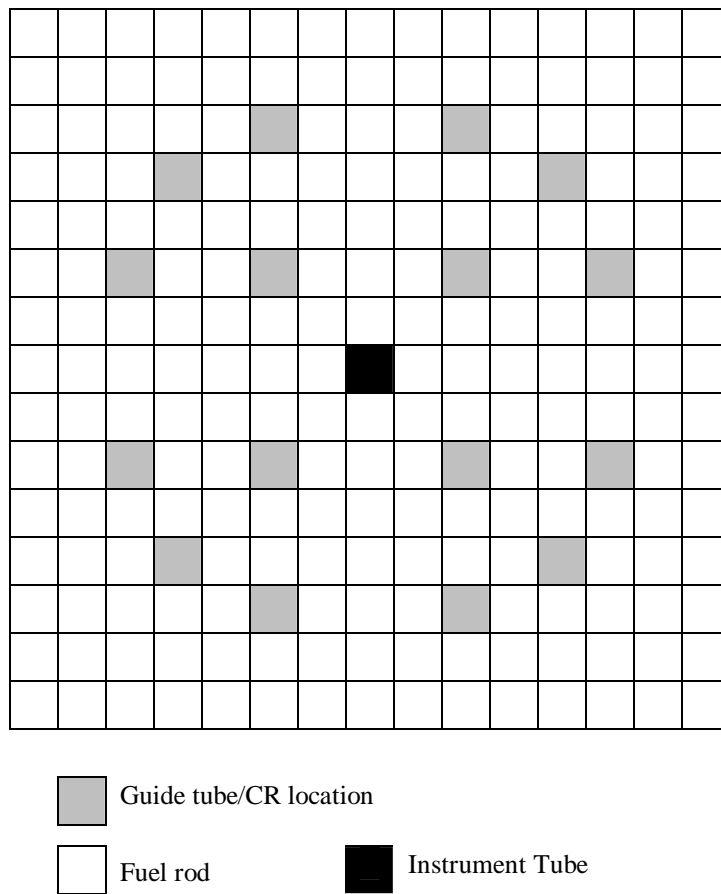


Figure 1 B&W 15 × 15 assembly lattice representing the CR locations

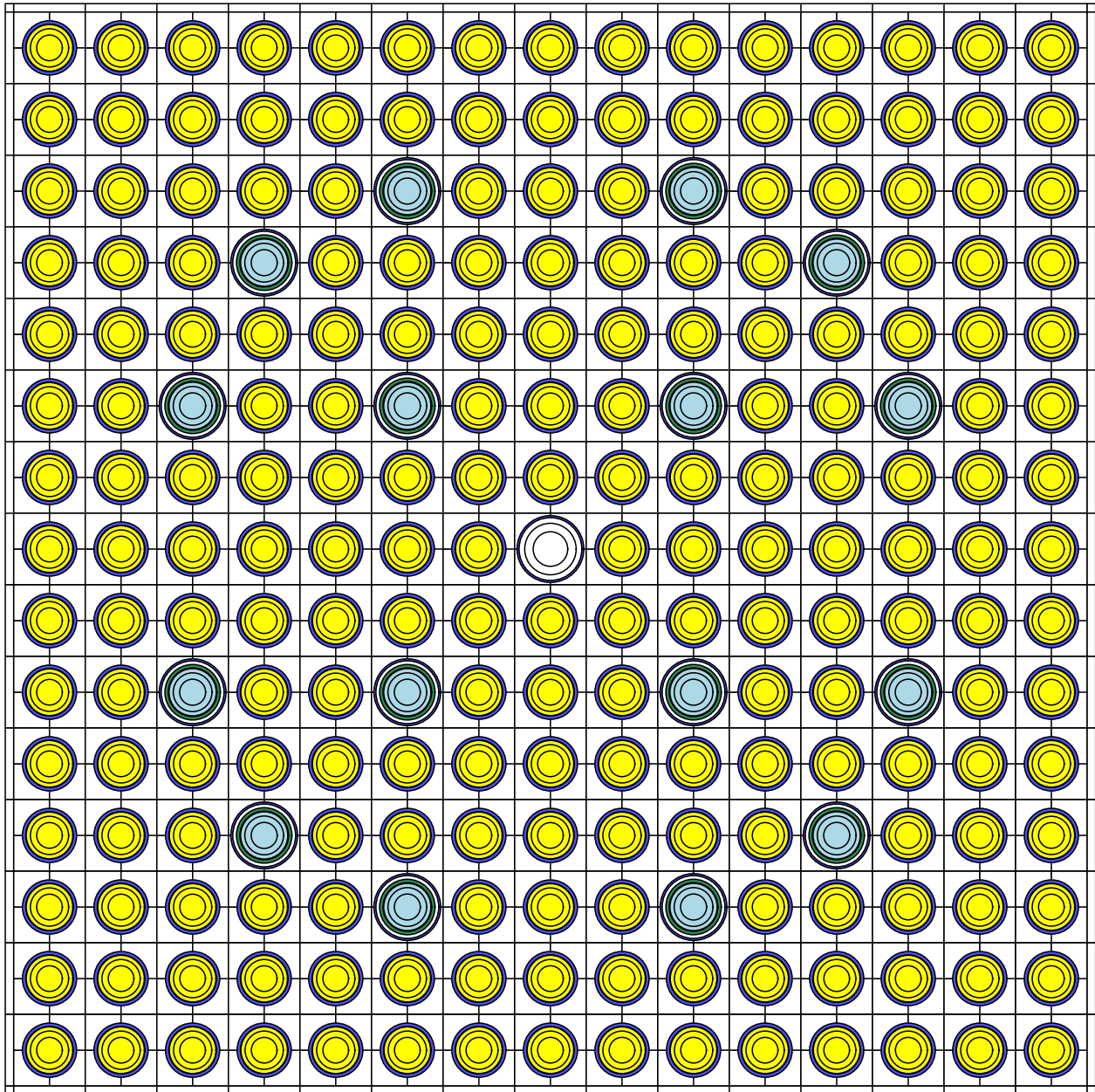


Figure 2 HELIOS calculational model of a B&W 15 × 15 assembly containing 16 CRs

The criticality calculations are performed for out-of-reactor conditions with isotopic compositions from the following conditions: (1) the uncontrolled condition (i.e., CRs not present during depletion) and (2) the controlled condition (i.e., CRs present during depletion). The k_{inf} values (out-of-reactor conditions) as a function of burnup from the two conditions are compared in Figure 3. The Δk values between these two conditions demonstrate the effect of CR exposure on reactivity.

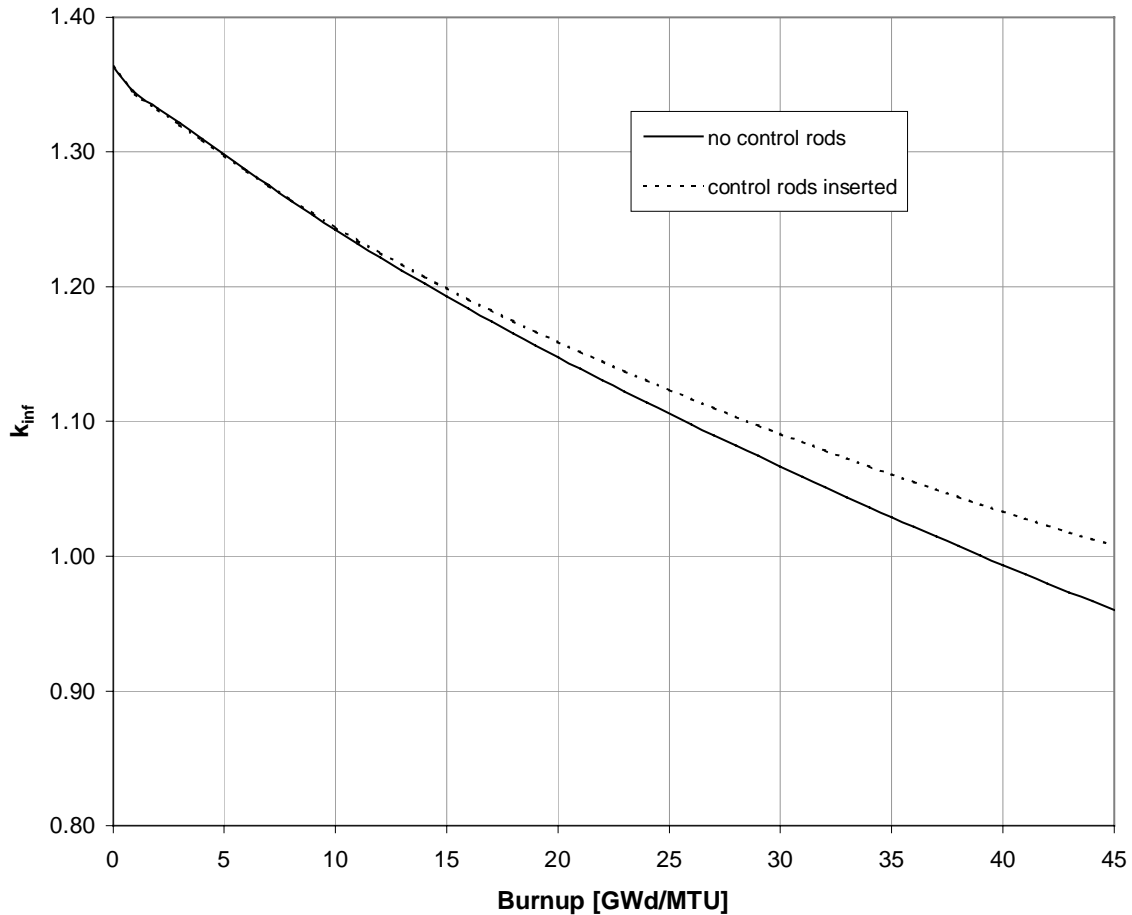


Figure 3 Comparison of k_{inf} values (out-of-reactor conditions) as a function of burnup. The results correspond to 4 wt % ^{235}U enriched B&W 15×15 fuel and Ag-In-Cd CRs.

For each of the following initial enrichments: 3, 4, and 5 wt % ^{235}U , calculations were performed for cases in which the CRs were withdrawn at 5, 15, 30, and 45 GWd/MTU (full exposure). Three cycles of 15 GWd/MTU per cycle were assumed for the analysis. The results (Δk as a function of burnup) are shown in Figure 4 for initial enrichments of 3, 4, and 5 wt % ^{235}U . It is evident from the figures that the reactivity effect of CRs increases with increasing exposure and decreasing fuel enrichment. These results are consistent with a previous study³ that examined the effect of BPR exposure on reactivity. The maximum positive Δk values for the various CR exposure cases considered are summarized in Table 3. For the cases considered here, the highest Δk is approximately 7% (the case when CRs are present during the entire depletion with 3 wt % ^{235}U enriched fuel).

When studying the Δk curves of the CRs a divergence in the behavior can be noted. This divergence appears at the moment when the CRs are withdrawn from the fuel assembly. A ‘bump’ appears because of the change in the rate at which Pu is being produced. When the CRs are withdrawn, the spectrum immediately softens because of the removal of strong absorbers. This causes a greater reactivity worth of ^{235}U , relative to that when CRs are present. Because the reactivity worth of ^{235}U is suddenly increased, the fission rate of ^{235}U increases as well. This effect is only temporary, and the fission rate will stabilize throughout the remainder of the depletion while the CRs are withdrawn. This ‘bump’ is more apparent at higher initial fuel enrichments. The increased reactivity effect at higher enrichment is because the reactivity worth of ^{235}U is less at 3 wt % enriched ^{235}U fuel than at 5 wt % enriched ^{235}U fuel. Consequently, the fission rates of ^{235}U will be higher at 5 wt % enriched fuel and the effects will be more apparent.

In addition to the calculations described above, the reactivity effect of CR exposure was studied for scenarios in which the CRs were inserted for a burnup duration of 5 GWd/MTU throughout the assembly burnup. The results (Δk as a function of burnup) are shown in Figure 5 for an initial enrichment of 4 wt % ^{235}U . Figure 5 show that CR exposure has a larger effect on discharge reactivity when it occurs later in the assembly burnup. Note that these calculations were performed to investigate/demonstrate the behavior, and may not represent realistic exposure conditions. However, some early U.S. PWR operations included significant CR insertions in conjunction with an assembly’s first burnup cycle.⁸ Thus, it is expected that cases involving exposure during the first cycle (i.e., within the first 15 GWd/MTU) are closer to reality than those involving exposure late in burnup.

Figure 6 compares the Δk for various initial fuel enrichments in which the CRs are present for the first 15 GWd/MTU (approximating 1 cycle). It is interesting to note that, following the initial jump, there is an increasing trend in the Δk values after the CRs are withdrawn for the cases with 4 and 5 wt % ^{235}U enrichment, but a decreasing trend for the 3 wt % ^{235}U enrichment case. While the CRs are inserted, they displace moderator and absorb thermal neutrons, significantly hardening the neutron spectrum. The hardened neutron spectrum results in reduced ^{235}U depletion, higher production of fissile plutonium isotopes and increased plutonium fission. Examination of the atom densities of ^{239}Pu and ^{235}U as a function of burnup reveals that the lower the initial ^{235}U enrichment, the greater the ^{239}Pu fission while the CRs are present. Therefore, lower initial ^{235}U enrichments have less net buildup of ^{239}Pu while the CRs are present (relative to higher initial ^{235}U enrichments), because they have an increased rate of ^{239}Pu fission during this period. When the CRs are withdrawn, the spectrum softens because of the removal of strong absorbers and added moderation. The reactivity worth of ^{235}U increases and consequently the fission rate increases. However, the higher initial ^{235}U enrichment cases have significantly more fissile plutonium built in relative to the case with no CR exposure. The increased fissile plutonium and subsequent increased plutonium fission result in a small degree of conversion, and thus there is an increase in Δk after the CRs have been withdrawn for the 4 and 5 wt % ^{235}U enriched cases. The reactivity worth of the 3 wt % ^{235}U enriched case is not increasing because, due to the lower initial ^{235}U enrichment, a significant portion of the ^{239}Pu is being depleted while the CRs are still present, which results in less net buildup of ^{239}Pu .

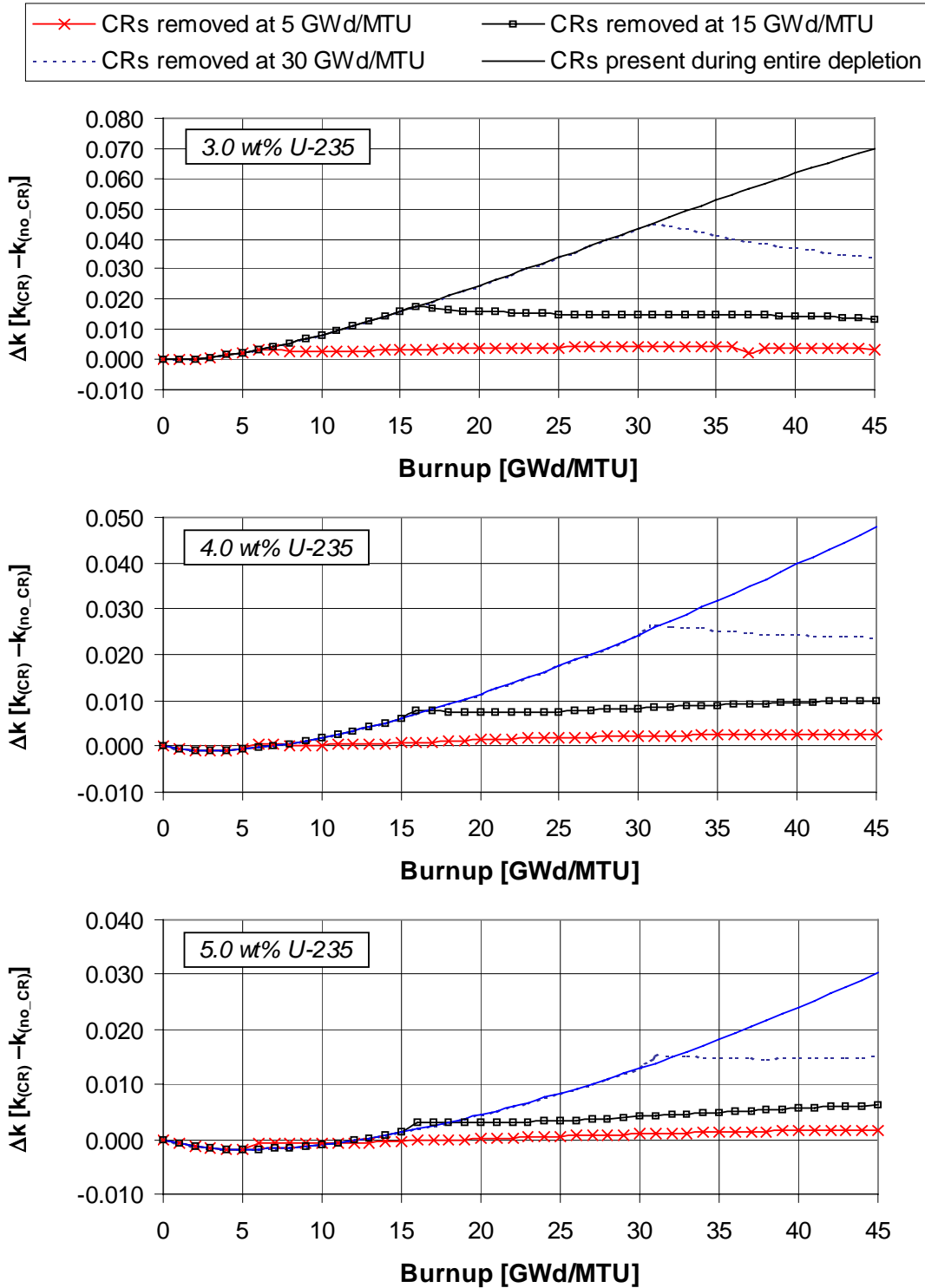


Figure 4 Comparison of Δk values as a function of burnup for various CR exposures with initial fuel enrichments of 3, 4, and 5 wt % ^{235}U , for B&W 15×15 fuel and Ag-In-Cd CRs

Table 3 Summary of maximum positive Δk values observed for B&W Ag-In-Cd CR cases considered (discharge burnup of 45 GWd/MTU)

Burnup at CR removal (GWd/MTU)	Enrichment (wt % ^{235}U)		
	3	4	5
5	0.0042	0.0026	0.0017
15	0.0177	0.0099	0.0063
30	0.0443	0.0266	0.0154
45	0.0697	0.048	0.0304

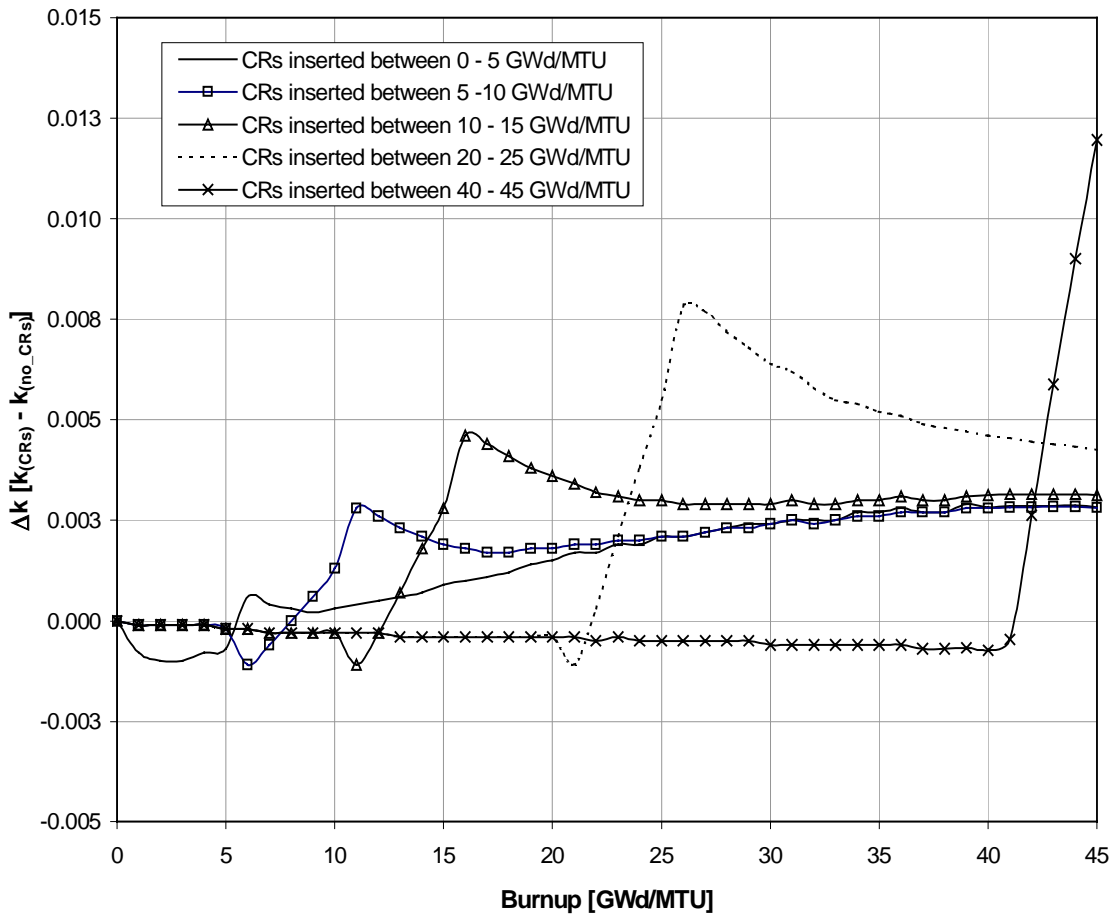


Figure 5 Comparison of Δk values as a function of burnup for 5 GWd/MTU CR exposures at various times during the burnup with 4 wt % ^{235}U B&W 15×15 fuel and Ag-In-Cd CRs

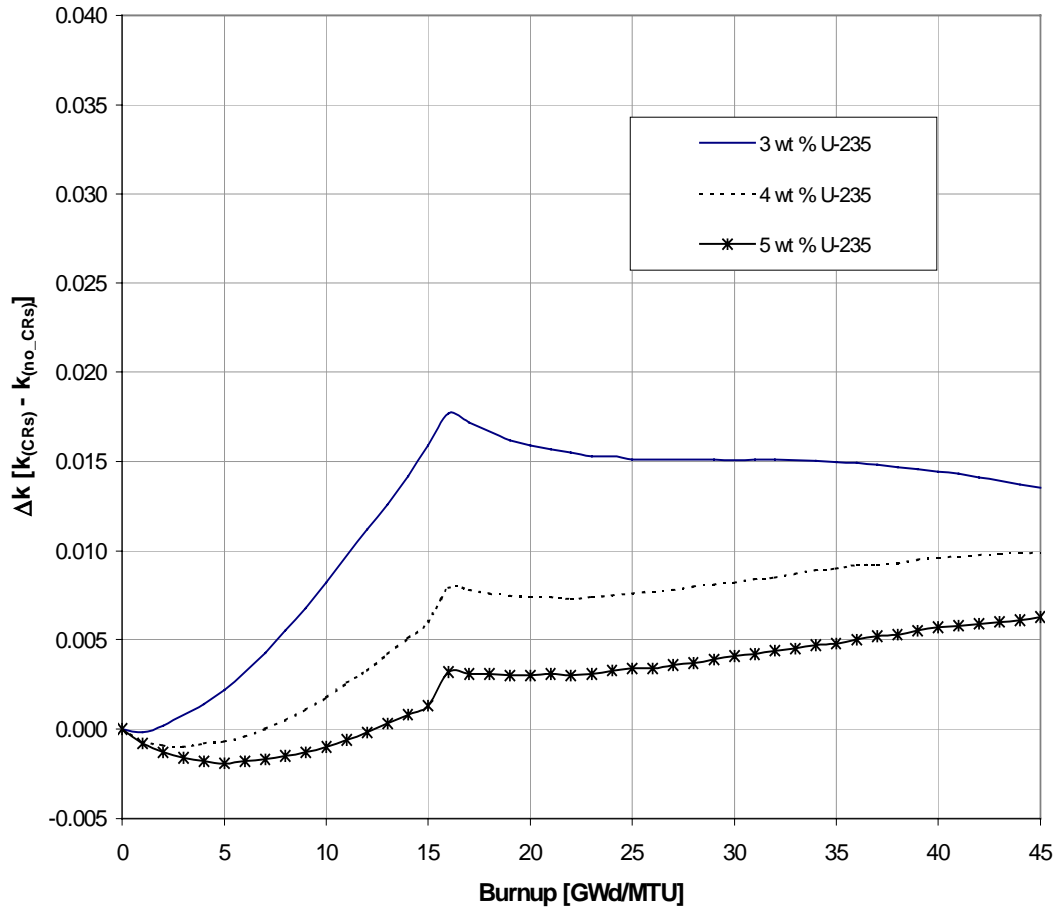


Figure 6 Comparison of Δk values as a function of burnup with CR exposure during the first 15 GWd/MTU (1 cycle) for various initial fuel enrichments. The results correspond to B&W 15×15 fuel and Ag-In-Cd CRs.

3.2.4 Westinghouse Hybrid Ag-In-Cd/B₄C Control Rods

The hybrid Ag-In-Cd/B₄C RCCA, developed by Westinghouse, consists of 24 Ag-In-Cd/B₄C CRs. Each CR contains Ag-In-Cd absorber with B₄C absorber pellets stacked on top of the Ag-In-Cd. Calculations were performed with a Westinghouse 17 × 17 assembly to investigate the reactivity effect of these CRs. Dimensional specifications for the fuel assembly and CRs are given in Table 4. The 17 × 17 Westinghouse assembly lattice is shown in Figure 7. Figure 8 displays the geometry of the Westinghouse 17 × 17 assembly as modeled in HELIOS-1.6.

Table 4 Westinghouse 17 × 17 fuel assembly and CR specifications

Parameter	Dimension (cm)
Fuel assembly specifications	
Rod pitch	1.2598
Assembly pitch	21.5
Cladding outside diameter	0.8898
Cladding inside diameter	0.8001
Pellet outside diameter	0.7844
Guide/instrument tube outside diameter	1.204
Guide/instrument tube inside diameter	1.123
Array size	17 × 17
Number of fuel rods	264
Number of guide/instrument tubes	25
Control rod specifications (Ref. 13)	
Absorber material	Natural B ₄ C/Ag-In-Cd
B ₄ C pellet diameter	0.84836
B ₄ C pellet axial height	259.08
Ag-In-Cd diameter	0.86614
Ag-In-Cd axial height	101.60
Cladding (304 SS) thickness	0.0470
Cladding inside diameter	0.87376
Cladding outside diameter	0.96774

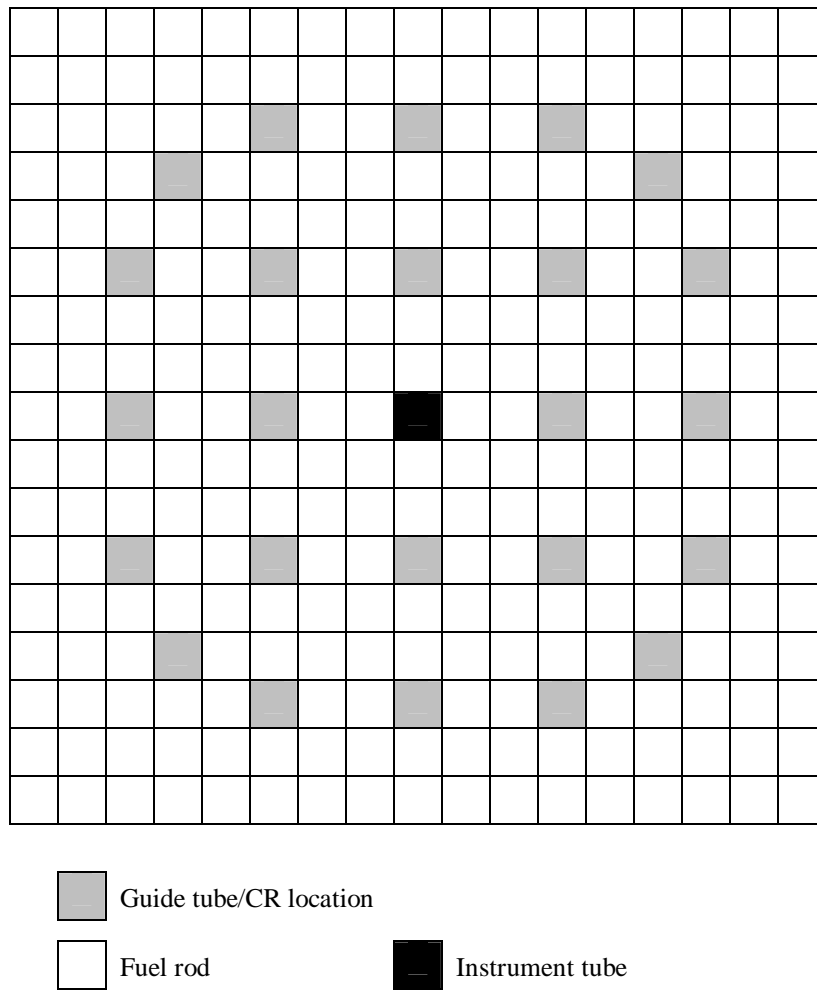


Figure 7 Westinghouse 17×17 assembly lattice representing the CR locations

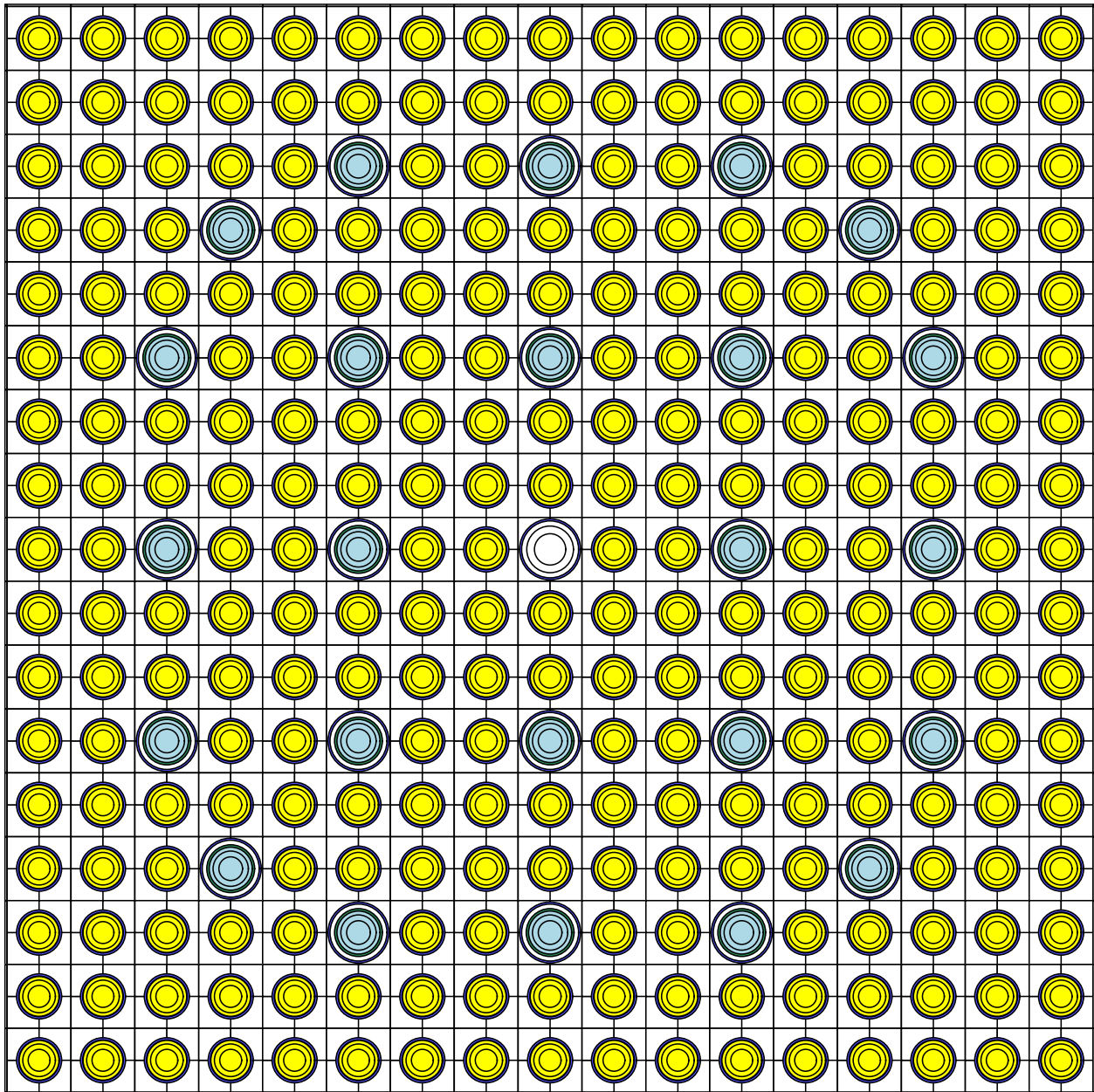


Figure 8 HELIOS calculational model of a Westinghouse 17×17 assembly containing 24 CRs

Analyses are presented in this section for the Westinghouse hybrid CR design with various initial fuel enrichments and various CR exposure conditions to better understand the effect of these CRs on reactivity. Since it is not possible to include the axial variation in absorber material in a 2-D model, separate models were developed to compare the effect of the two-absorber materials. The first model represented the axial segment of the CR corresponding to the B_4C region, while the second model represented the axial segment of the CR corresponding to the Ag-In-Cd region. The k_{inf} values, as a function of burnup from calculations with and without CR exposure, are compared in Figure 9. The Δk values between these conditions demonstrate the effect of these CRs on

reactivity and that the B₄C region of the CR results in a larger positive reactivity effect, as compared to the Ag-In-Cd region. Since the effect of Ag-In-Cd CRs was demonstrated in the previous section with B&W fuel, the remainder of the calculations in this section will involve the axial segment corresponding to the B₄C region. Note, however, that the lower ~100 cms of these CRs contain Ag-In-Cd, and thus partial CR insertions may only involve the Ag-In-Cd region.

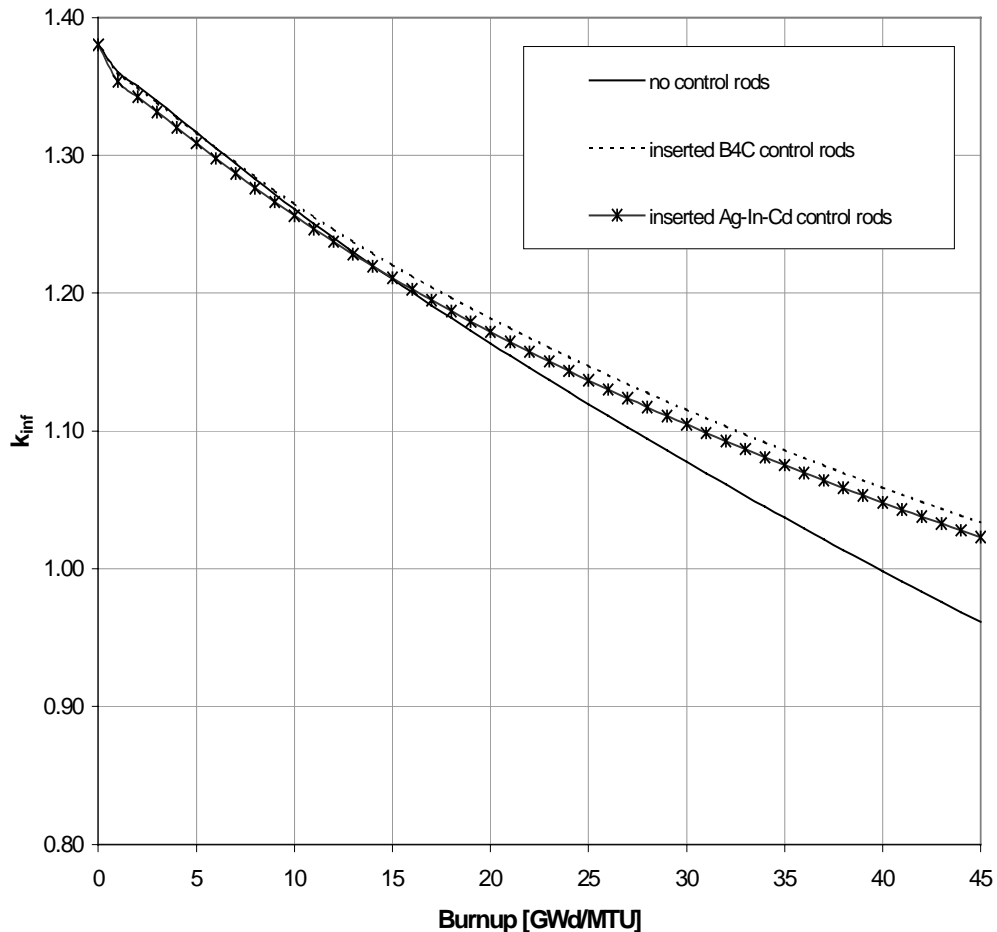


Figure 9 Comparison of k_{inf} values (out-of-reactor conditions) as a function of burnup with and without CR exposure. The results correspond to 4 wt % ²³⁵U enriched Westinghouse 17 × 17 fuel and Ag-In-Cd/B₄C CRs.

Calculations were performed with initial enrichments of 3, 4, and 5 wt % ^{235}U and CR exposures of 5, 15, 30, and 45 GWd/MTU (full exposure). Three cycles of 15 GWd/MTU per cycle were assumed for the analysis. The results (Δk as a function of burnup) are shown in Figure 10 for initial enrichments of 3, 4, and 5 wt % ^{235}U . Consistent with the results shown in the previous section, the reactivity effect of the CRs increases with increasing exposure and decreasing fuel enrichment. Note, however, the larger reactivity effect of B_4C absorber, relative to the Ag-In-Cd absorber considered in the previous section. The maximum positive Δk values for the various CR cases considered are summarized in Table 5. For the cases considered here, the highest Δk is approximately 10% (the case when CRs are present during the entire depletion with 3 wt % ^{235}U enriched fuel).

In addition to the calculations described above, the reactivity effect was studied for scenarios in which the CRs were inserted for a burnup duration of 5 GWd/MTU throughout the assembly burnup. The results (Δk as a function of burnup) are shown in Figure 11 for an initial enrichment of 4 wt % ^{235}U . Consistent with the results shown in the previous section, this figure shows that CR exposure has a larger effect on discharge reactivity when it occurs later in the assembly burnup.

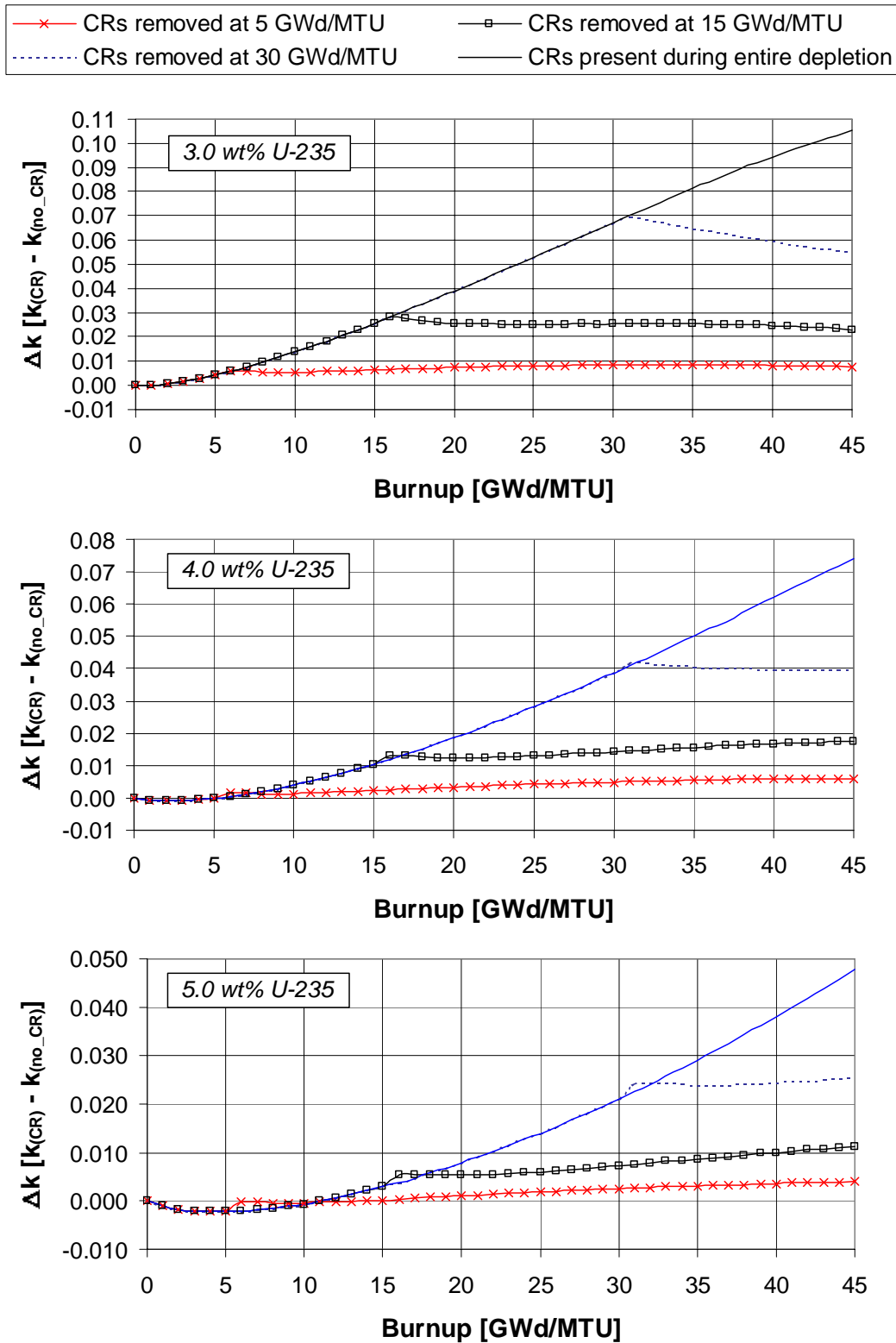


Figure 10 Comparison of Δk values as a function of burnup for various CR exposures with initial fuel enrichments of 3, 4, and 5 wt % ^{235}U . The results correspond to Westinghouse 17×17 fuel and the B_4C axial segment of the hybrid Ag-In-Cd/ B_4C CRs.

Table 5 Summary of maximum positive Δk values observed for B₄C axial segment of the Westinghouse hybrid Ag-In-Cd/B₄C CR cases considered (discharge burnup of 45 GWd/MTU)

Burnup at CR removal (GWd/MTU)	Enrichment (wt % ²³⁵ U)		
	3.0	4.0	5.0
5	0.0086	0.0048	0.0041
15	0.0280	0.0174	0.0113
30	0.0698	0.0417	0.0256
45	0.1050	0.0739	0.0479

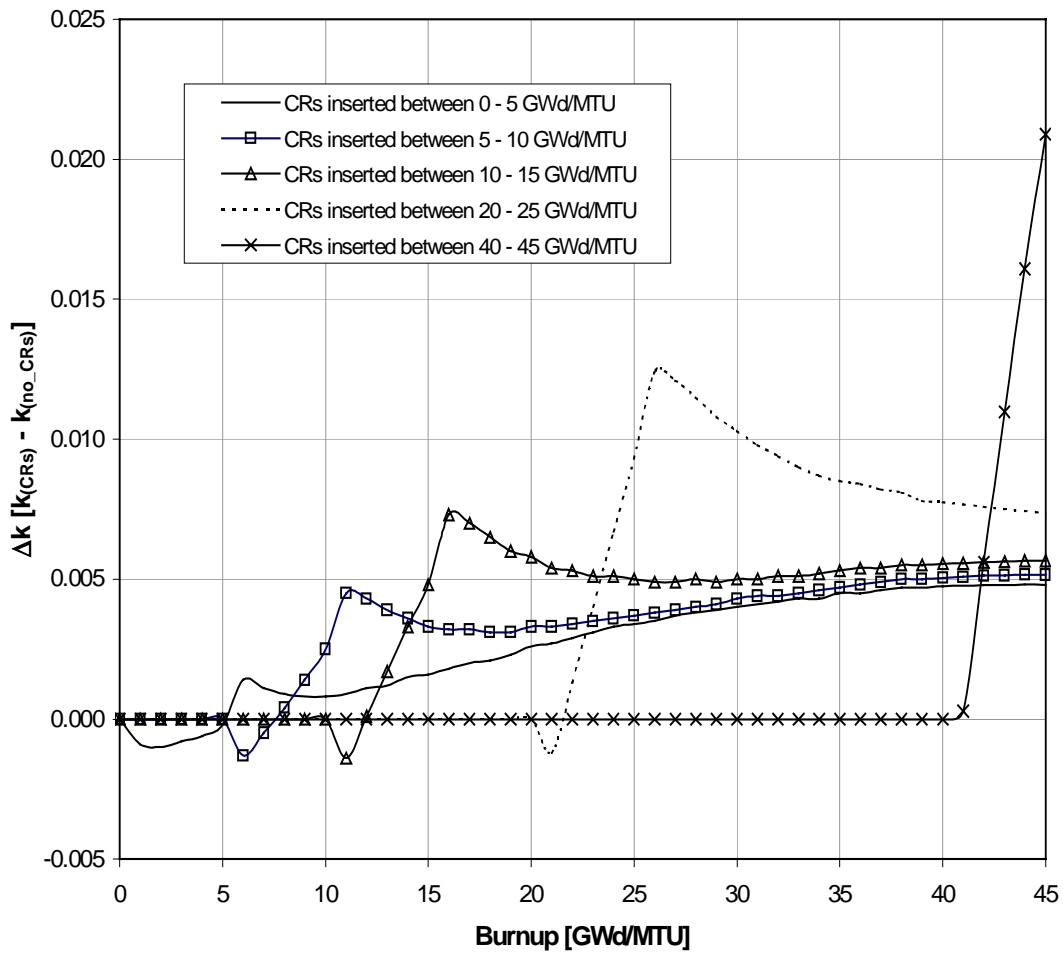


Figure 11 Comparison of Δk values as a function of burnup for 5 GWd/MTU CR exposures at various times during the burnup with initial fuel enrichment of 4 wt % ²³⁵U. The results correspond to Westinghouse 17 × 17 fuel and B₄C CRs.

3.2.5 CE Ag-In-Cd/B₄C Control Rods

Combustion Engineering has designed a CEA consisting of five Inconel fingers loaded with a stack of B₄C cylindrical pellets, with Ag-In-Cd in the lower 8 in. (20.32 cm) of the fingers. Calculations are presented in this section to investigate the reactivity effect of these CE CRs within a CE 14 × 14 fuel assembly design. Dimensional specifications for the fuel assembly and CRs used for this analysis are given in Table 6 (Ref. 12). The 14 × 14 CE assembly lattice is shown in Figure 12, and Figure 13 displays the assembly as modeled in HELIOS-1.6.

Table 6 CE 14 × 14 fuel assembly and CR specifications

Parameter	Dimension (cm)
Fuel assembly specifications	
Rod pitch	1.47
Assembly pitch	20.8
Cladding outside diameter	1.1176
Cladding inside diameter	0.97536
Pellet outside diameter	0.95631
Guide tube outside diameter	2.6289
Guide tube inside diameter	2.8321
Array size	14 × 14
Number of fuel rods	176
Number of guide/instrument tubes	5
Control rod specifications	
Absorber material	Natural B ₄ C/Ag-In-Cd
B ₄ C pellet diameter	2.1844
B ₄ C axial height	340.36 (center finger) / 314.96 (outside fingers)
Ag-In-Cd diameter	2.1844
Ag-In-Cd axial height	20.32
Cladding (Inconel) thickness	0.1016
Cladding outside diameter	2.4079

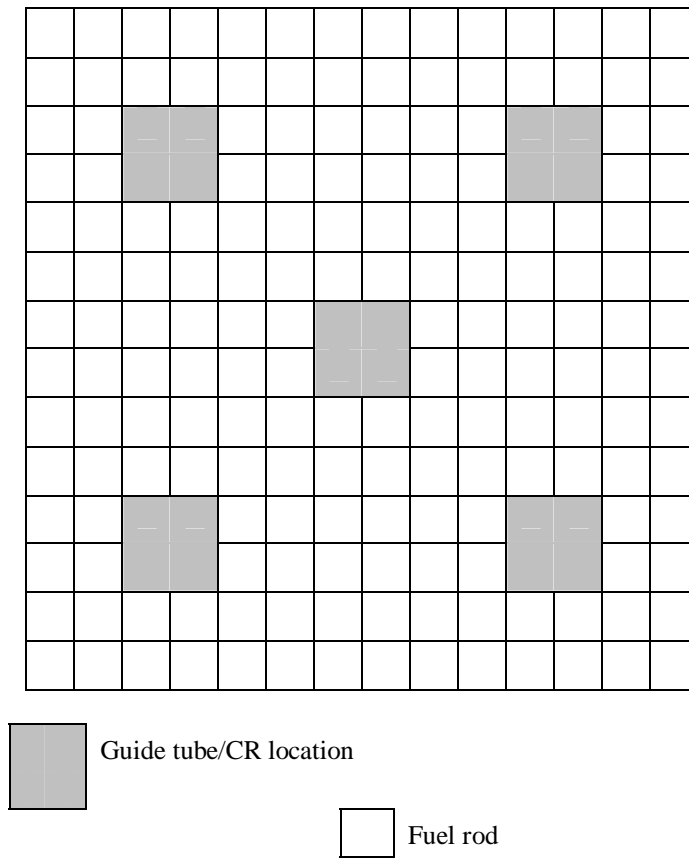


Figure 12 CE 14×14 assembly lattice representing the CR locations

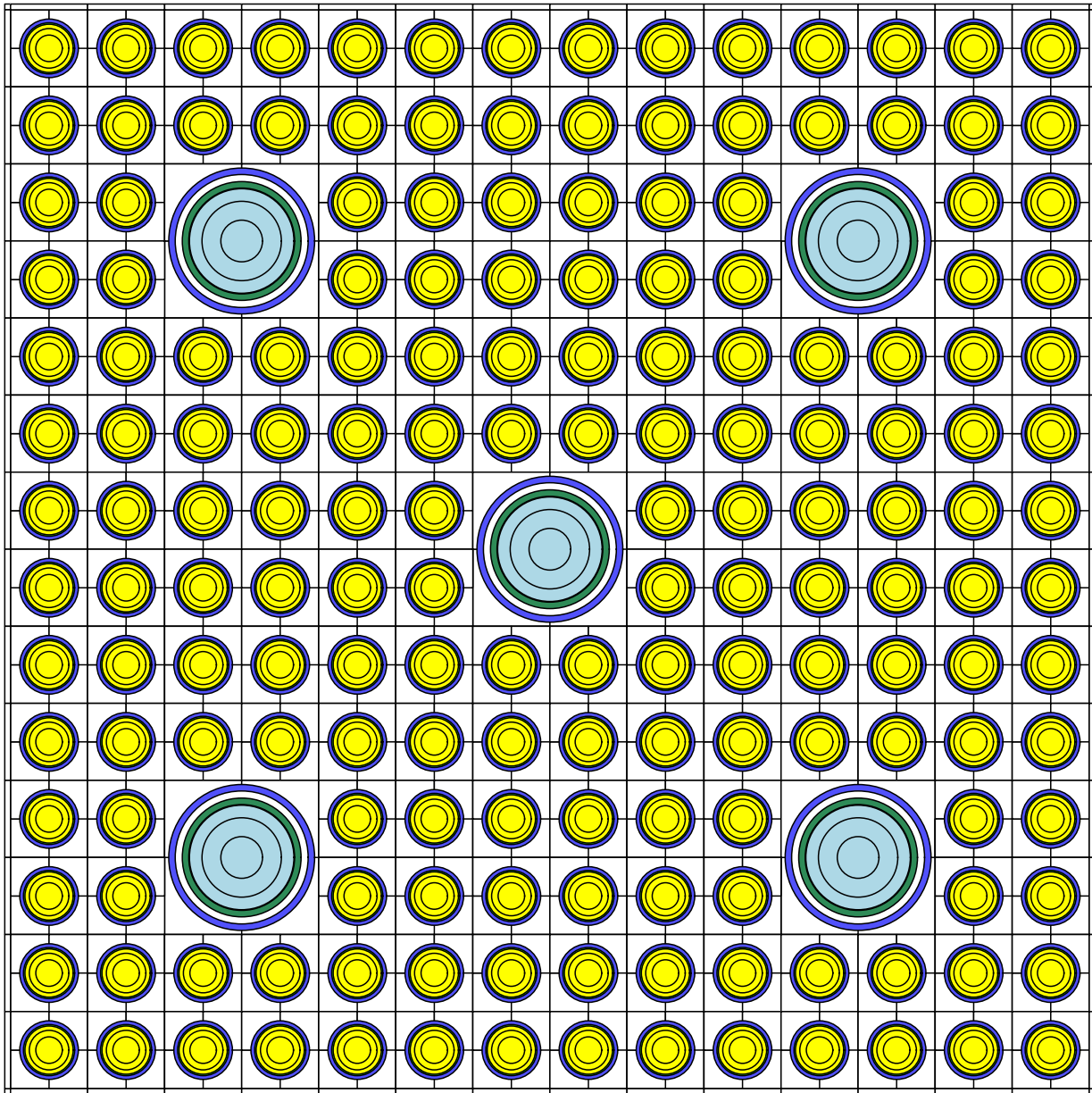


Figure 13 HELIOS calculational model of a CE 14×14 assembly containing five CRs

Analyses are presented in this section for the CE CEA with various initial fuel enrichments and CR exposures to better understand the effect of these CRs on the reactivity of SNF. Since the primary material in these CRs is B_4C , and it is not possible to include the axial variation in absorber materials in a 2-D model, the calculations in this section involve the axial segment corresponding to the B_4C region. Based on results shown in the previous sections, calculations with the Ag-In-Cd axial segment are expected to yield smaller effects. Note however, that the lower ~ 20 cm of these CRs contain Ag-In-Cd, and thus, partial CR insertions may only involve the Ag-In-Cd region. Figure 14 displays the k_{inf} values versus burnup from calculations with and without CR exposure.

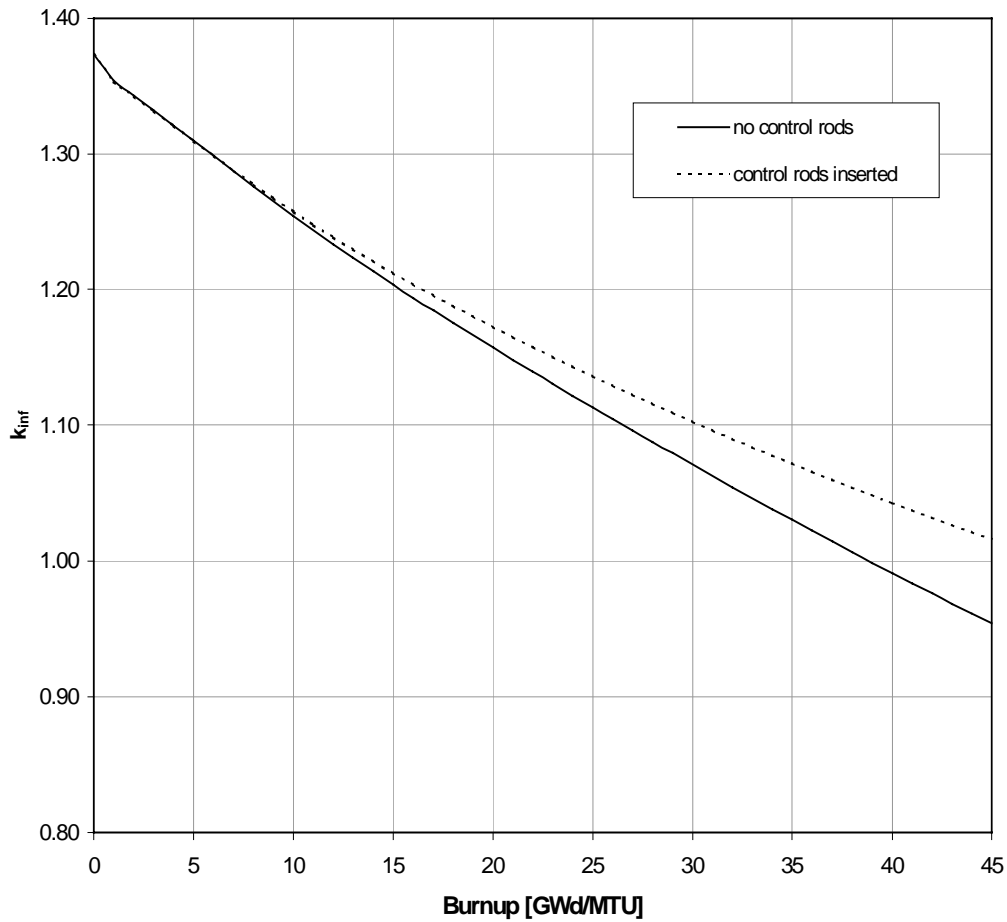


Figure 14 Comparison of k_{inf} (out-of-reactor conditions) as a function of burnup with and without CR exposure. The results correspond to 4 wt % ^{235}U enriched CE 14×14 fuel and the B_4C axial segment of the Ag-In-Cd/ B_4C CRs.

Consistent with the analyses in the previous sections, calculations were performed with initial enrichments of 3, 4, and 5 wt % ^{235}U and CR exposures of 5, 15, 30, and 45 GWd/MTU (full exposure). Three cycles of 15 GWd/MTU per cycle were assumed for the analysis. The results (Δk as a function of burnup) are shown in Figure 15 for initial enrichments of 3, 4, and 5 wt % ^{235}U . The maximum positive Δk values for the various CR cases considered are summarized in Table 7. For the cases considered here, the highest Δk is approximately 9% (the case when CRs are present during the entire depletion at 3 wt % ^{235}U fuel enrichment). Consistent with the results shown in the previous sections, the reactivity effect of the CRs increases with increasing exposure and decreasing fuel enrichment.

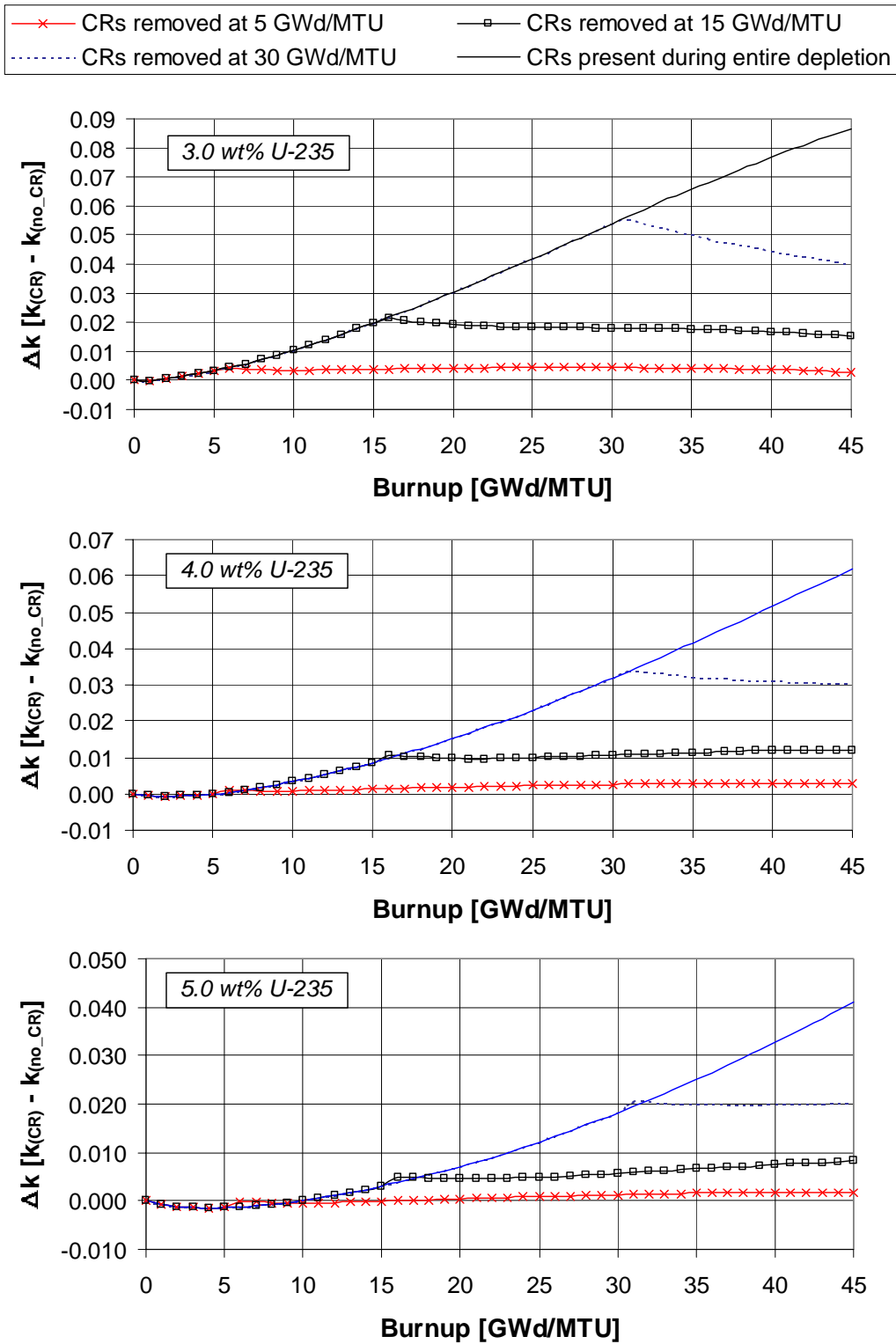


Figure 15 Comparison of Δk values as a function of burnup for various CR exposures with initial fuel enrichments of 3, 4, and 5 wt % ^{235}U . The results correspond to CE 14×14 fuel and the B_4C axial segment of the Ag-In-Cd/ B_4C CRs.

Table 7 Summary of maximum positive Δk values observed for the B₄C axial segment of the CE Ag-In-Cd/B₄C CR cases considered (discharge burnup of 45 GWd/MTU)

Burnup at CR removal (GWd/MTU)	Enrichment (wt % ²³⁵ U)		
	3.0	4.0	5.0
5	0.0045	0.0028	0.0018
15	0.0213	0.0121	0.0082
30	0.0553	0.0339	0.0203
45	0.0866	0.0619	0.0411

3.2.6 B&W Gray Axial Power Shaping Rods

In addition to the Ag-In-Cd CRs analyzed in Section 3.2.3, B&W has developed gray part-length APSRs made out of Inconel with stainless steel cladding (the balance of the length is filled with water). Note that B&W has also developed black part-length APSRs made out of Ag-In-Cd with stainless steel cladding. However, the black APSRs are not being analyzed in this report due to their similarity with the Ag-In-Cd CRs (Section 3.2.3). Calculations were performed using a B&W 15 × 15 assembly in order to investigate the reactivity effect of the gray APSRs. Dimensional specifications for the fuel assembly and APSRs are given in Table 8 (Ref. 11). The B&W 15 × 15 assembly design considered is shown in Figure 16.

As in the previous CR studies, various rod exposures were considered in order to better understand the effect these power shaping rods have on reactivity as a function of burnup. In reality, the APSRs are shorter than the active fuel length. However, this analysis is done in 2-D and consequently the APSRs and the active fuel are both infinite lengthwise. The k_{inf} values, as a function of burnup from the calculations with and without APSR exposure are compared in Figure 17. The Δk values between these two conditions demonstrate the effect of APSRs on reactivity.

Calculations were performed with initial enrichments of 3, 4, and 5 wt % ²³⁵U and APSRs exposures of 5, 15, 30, and 45 GWd/MTU (full exposure). Three cycles of 15 GWd/MTU per cycle were assumed for the analysis. The results (Δk as a function of burnup) are shown in Figure 18 for initial enrichments of 3, 4, and 5 wt % ²³⁵U. The maximum positive Δk values for the various APSR cases considered are summarized in Table 9. For the cases considered here the highest Δk is approximately 2.7 % Δk (the case when APSRs are present during the entire depletion at 3 wt % ²³⁵U fuel enrichment), which is significantly less than the 7–10% Δk observed for the other CR designs. Consistent with the results shown in previous sections for other CR designs, the reactivity effect of the APSRs increases with increasing exposure and decreasing fuel enrichment. Note, however, that the APSRs have a significantly smaller reactivity effect compared to the other CR designs considered in this report; this is because the APSRs do not contain strong thermal neutron absorbing materials such as boron or cadmium.

Figure 19 compares the Δk for various initial fuel enrichment cases in which the APSRs have been inserted for 30 GWd/MTU (representing 2 cycles). As noted previously, the reactivity effect of the APSRs increases with decreasing initial enrichment.

Based on a limited survey of operational data, it is difficult to characterize “typical” APSR operational practices. However, it is often the case that they are present during the majority of an assembly’s second burnup cycle, being withdrawn gradually late in the cycle.¹¹ Therefore, calculations were performed for scenarios in which the APSRs were inserted during the first (0–15 GWd/MTU), second (15–30 GWd/MTU), and third (30–45 GWd/MTU) cycle of burnup to quantify the reactivity effect. The results (Δk as a function of burnup) are shown in Figure 20 for an initial enrichment of 4.0 wt % ²³⁵U and demonstrate that, consistent with the results shown previously for CRs, the APSR exposure has a larger effect on discharge reactivity when it occurs later in the assembly burnup.

Table 8 B&W 15 × 15 fuel assembly and APSR specifications

Parameter	Dimension (cm)
Fuel assembly specifications	
Rod pitch	1.44272
Assembly pitch	21.81
Cladding outside diameter	1.09220
Cladding inside diameter	0.95758
Pellet outside diameter	0.940
Guide/instrument tube outside diameter	1.34620
Guide/instrument tube inside diameter	1.26492
Array size	15 × 15
Number of fuel rods	208
Number of guide/instrument tubes	17
APSR specifications	
Rod material	Inconel
Inconel outer diameter	0.95250
Inconel axial height	160.02
Cladding (304 SS) outside diameter	1.11760
Cladding (304 SS) inside diameter	0.98044

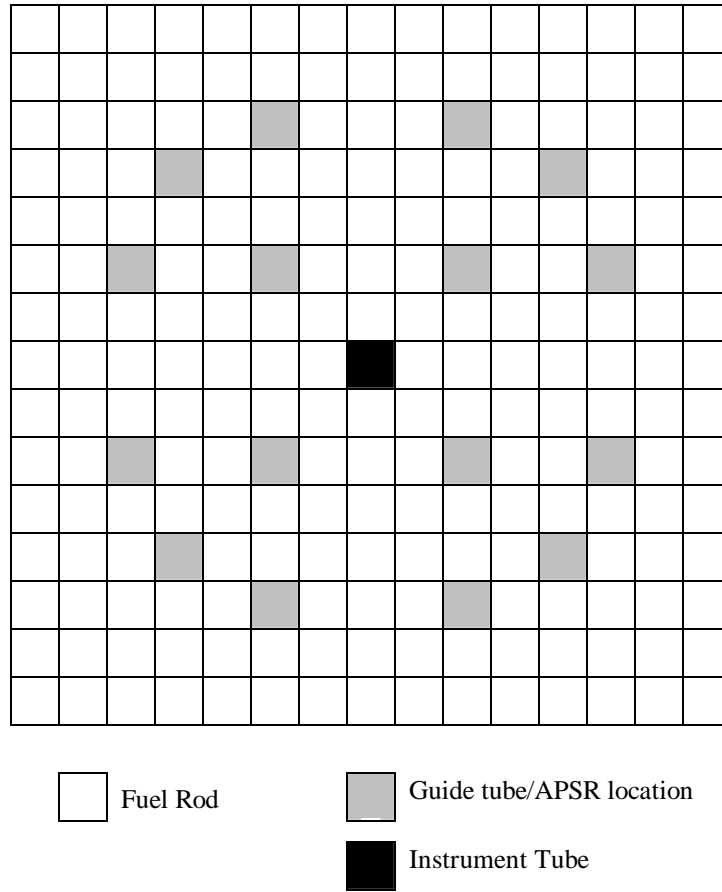


Figure 16 B&W 15 × 15 assembly lattice representing the APSRS locations

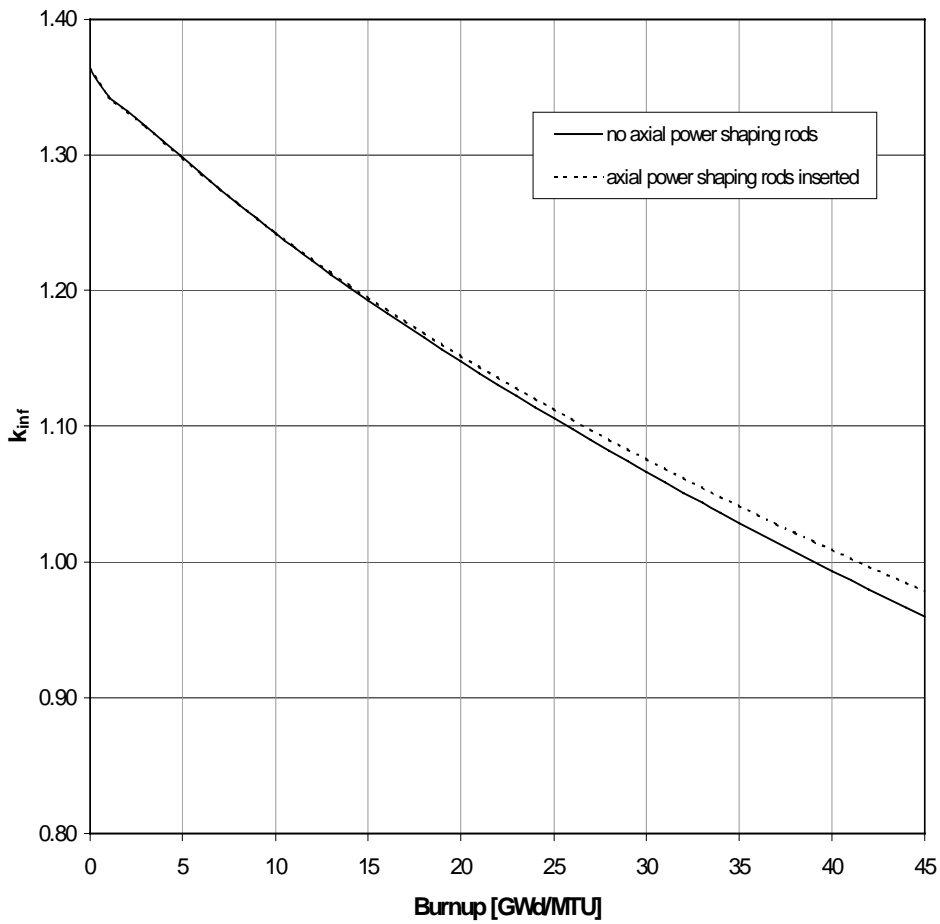


Figure 17 Comparison of k_{inf} values (out-of-reactor conditions) as a function of burnup with and without APSR exposure. The results correspond to 4 wt % ^{235}U enriched B&W 15×15 fuel and gray APSRs.

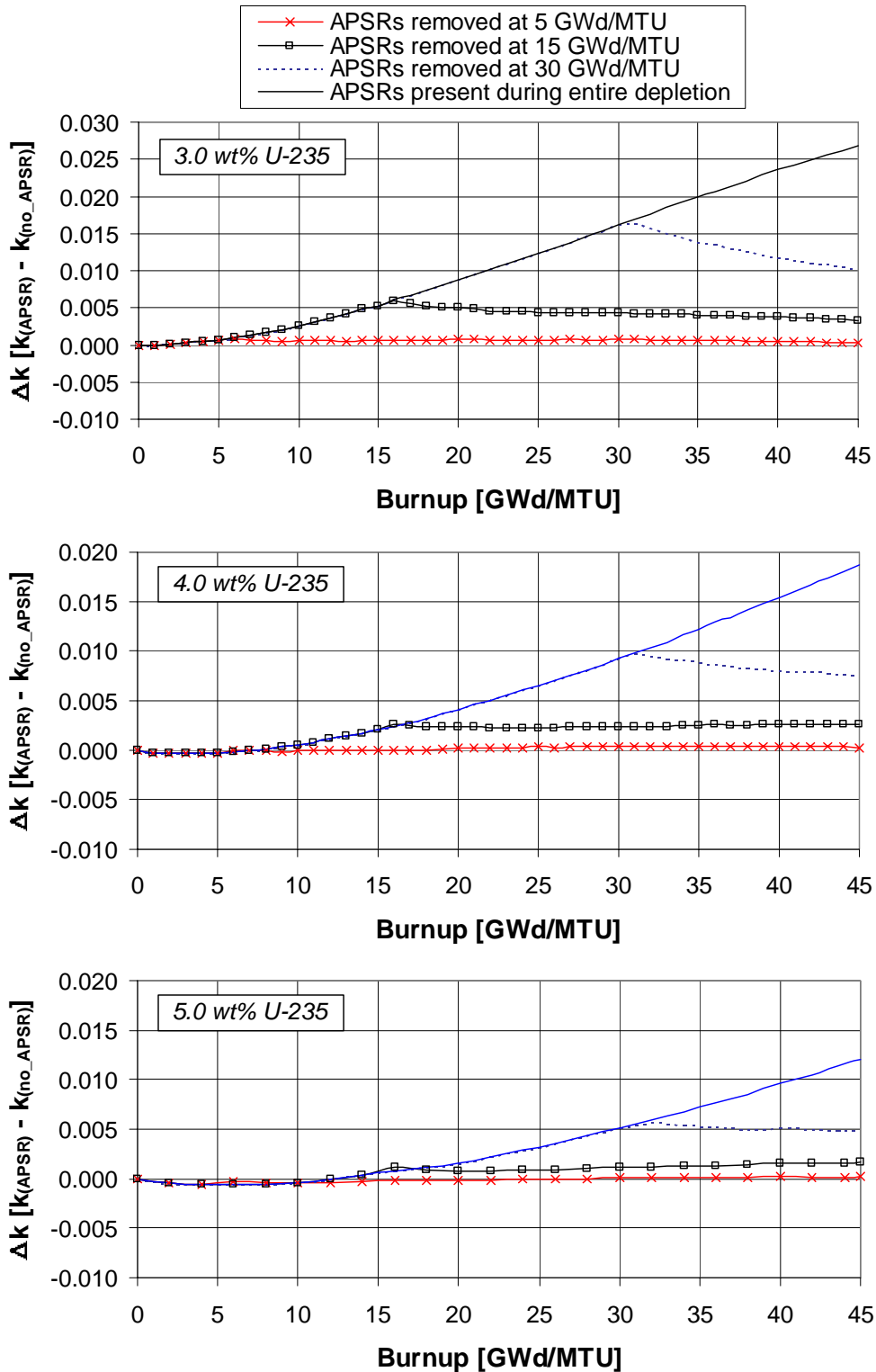


Figure 18 Comparison of Δk values as a function for various APSR exposures with initial fuel enrichments of 3, 4, and 5 wt % ^{235}U . The results correspond to B&W 15×15 fuel and gray APSRs.

Table 9 Summary of maximum positive Δk values observed for B&W APSR cases considered (discharge burnup of 45 GWd/MTU)

Burnup at CR removal (GWd/MTU)	Enrichment (wt % ^{235}U)		
	3.0	4.0	5.0
5	0.0008	0.0004	0.0002
15	0.0059	0.0026	0.0017
30	0.0164	0.0098	0.0057
45	0.0268	0.0187	0.0121

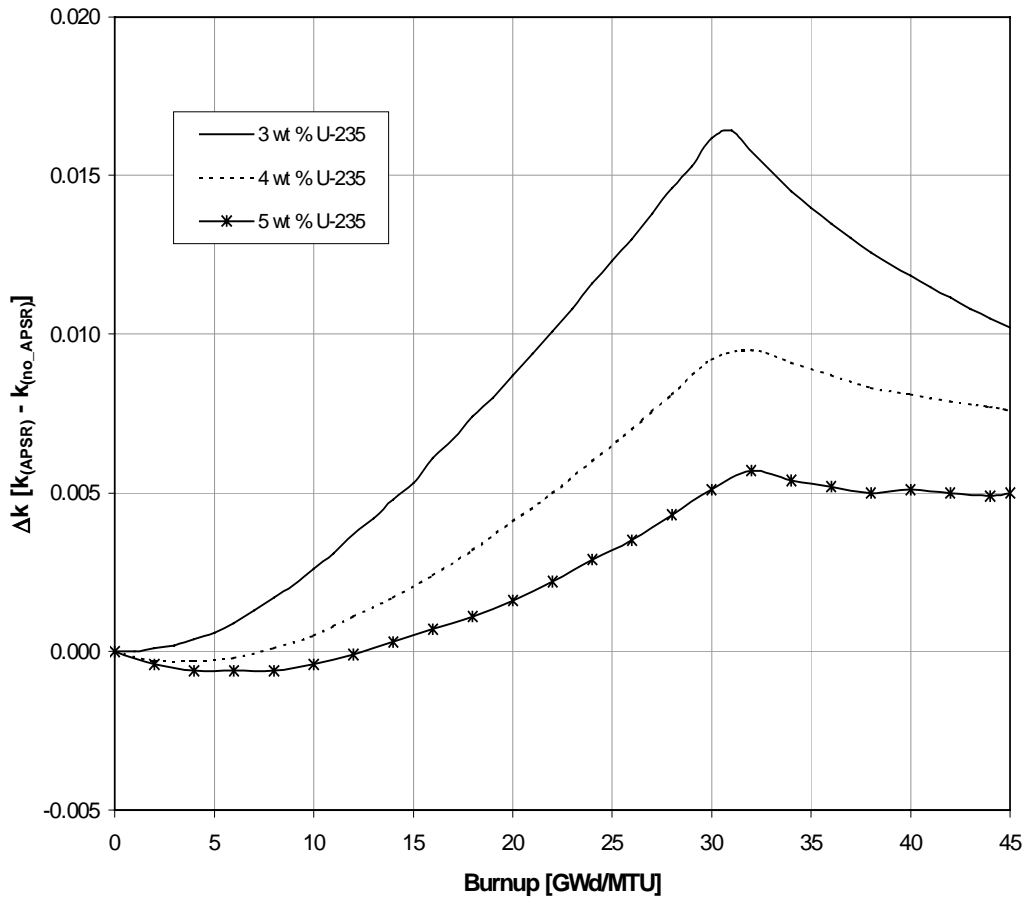


Figure 19 Comparison of Δk values as a function of burnup with APSR exposure during the first 30 GWd/MTU (2 cycles) for various initial fuel enrichments. The results correspond to B&W 15×15 fuel and gray APSRs.

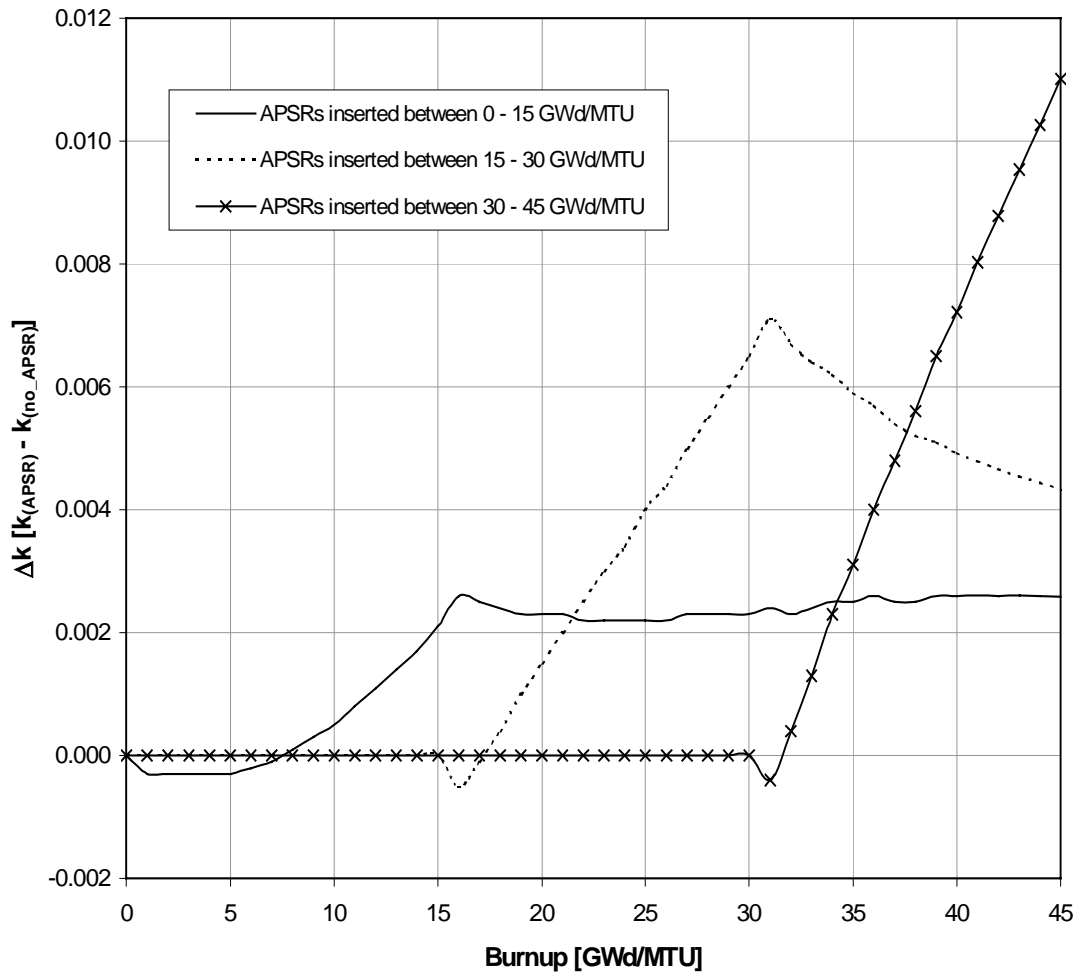


Figure 20 Comparison of Δk values as a function of burnup for 15 GWd/MTU APSR exposures at various times during the burnup with initial fuel enrichment of 4 wt % ^{235}U . The results correspond to B&W 15×15 fuel and gray APSRs.

3.2.7 Cooling Time

To study the effects of cooling time, a few calculations were performed at cooling times other than zero. The Westinghouse 17×17 fuel assembly and the Ag-In-Cd/B₄C CRs were employed for the study. Infinite assembly array calculations were performed for cooling times of 5, 20, and 40 years with initial fuel enrichment of 4 wt % ^{235}U and CR exposure of 45 GWd/MTU (full exposure). The results (Δk as a function of burnup) are shown in Figure 21. It can be seen that cooling time has little impact on the Δk values, and thus, the results at zero cooling time are expected to be representative within the time frame relevant to cask storage and transport.

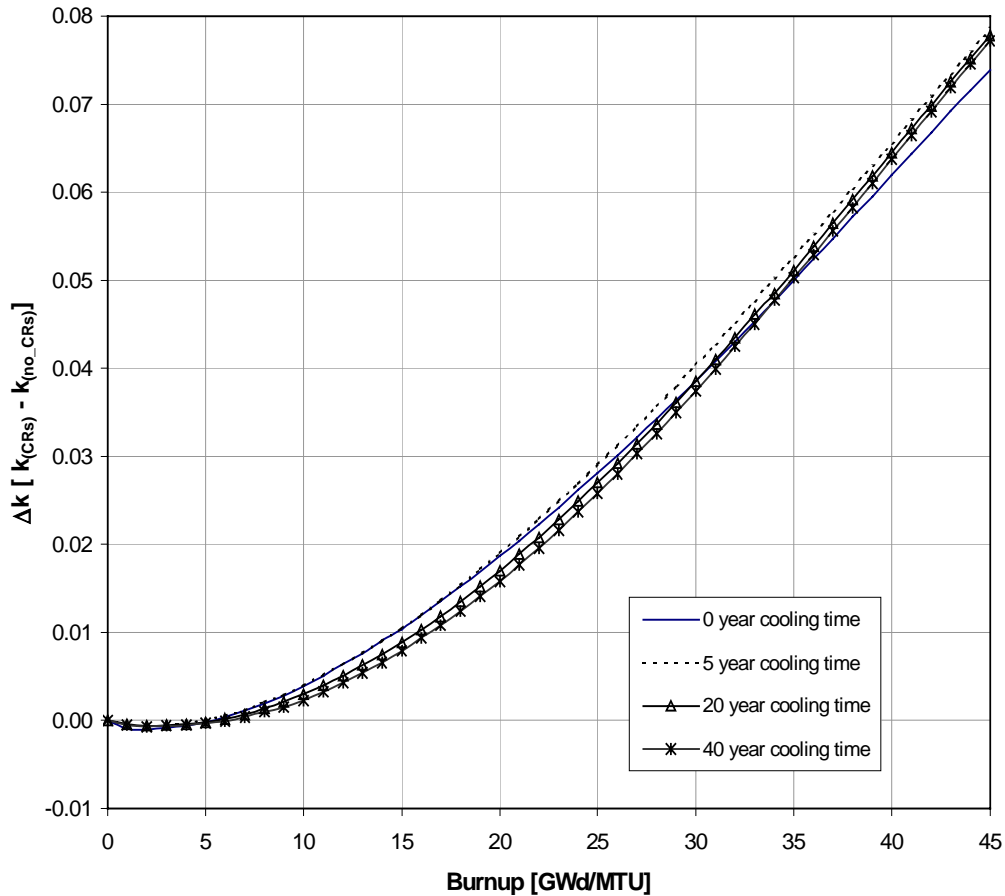


Figure 21 Comparison of Δk values as a function of burnup for various cooling times for 45 GWd/MTU CR exposures with initial fuel enrichment of 4 wt % ^{235}U . The results correspond to Westinghouse 17×17 fuel and the B_4C segment of the Ag-In-Cd/ B_4C CRs.

3.2.8 Summary of Two-Dimensional Analyses

It can be concluded from the analyses in this subsection that the reactivity effect of CR insertion increases with increasing exposure and decreasing fuel enrichment. The gray APSRs showed similar trends to CRs, although the reactivity effects were not as pronounced for the APSRs. For a discharge burnup of 45 GWd/MTU, the CRs showed maximum (worst-case) Δk values between 7–10%, while the APSRs had maximum Δk values around 2–3%. When considering these quoted “maximum Δk values,” the reader should be mindful that they are based on calculational assumptions selected to bound the reactivity effect (i.e., full axial CR insertion during the entire burnup), and not realism of operations. A summary and comparison of Δk values for the various CR designs and burnup exposures considered are shown in Figure 22. To gain an understanding of the reactivity effect of CRs on SNF loaded in a burnup credit cask and the reactivity effect of partially inserted CRs, 3-D cask calculations are presented in the following section

Regarding the effect of the various CR designs considered, it is noted that there exists a direct relationship between the initial reactivity worth of a CR design and its effect on the discharge reactivity – higher reactivity worth CR designs result in larger effects on discharge reactivity. To examine this relationship, the effect of CR

exposure on discharge reactivity (in terms of Δk) was plotted against the CR initial reactivity worth (in terms of $\Delta k/k$) for each of the CR and APSR designs considered. The relationship is plotted in Figure 23 for cases involving fuel with 45 GWd/MTU burnup and 4.0 wt % ^{235}U initial enrichment that have experienced different CR exposure durations. The results in Figure 23 show that the positive reactivity effect of CRs on discharged SNF increases in a linear manner with increasing negative CR reactivity worth. Note that the CR reactivity worth was determined based on criticality calculations with and without the CRs/APSRs present for in-reactor conditions and zero burnup, while the reactivity effect on the discharged SNF is based on criticality calculations in out-of-reactor conditions (without CRs/APSRs present) with isotopic compositions from depletion cases with and without CRs/APSRs present.

Besides establishing a relationship between the initial CR reactivity worth and the reactivity effect on discharged SNF, Figure 23 could be used as a guide for estimating the reactivity effect of other CR and APSR designs that are not included in this report. For example, calculations were performed for Westinghouse Hf CRs and Westinghouse Ag-In-Cd-CRs with 4 wt % ^{235}U enriched Westinghouse 17×17 fuel and 5 and 45 GWd/MTU CR exposures. The results are included on Figure 23 to demonstrate that the calculated reactivity effect of these additional CRs is consistent with that predicted by the 5 and 45 GWd/MTU lines displayed in Figure 23.

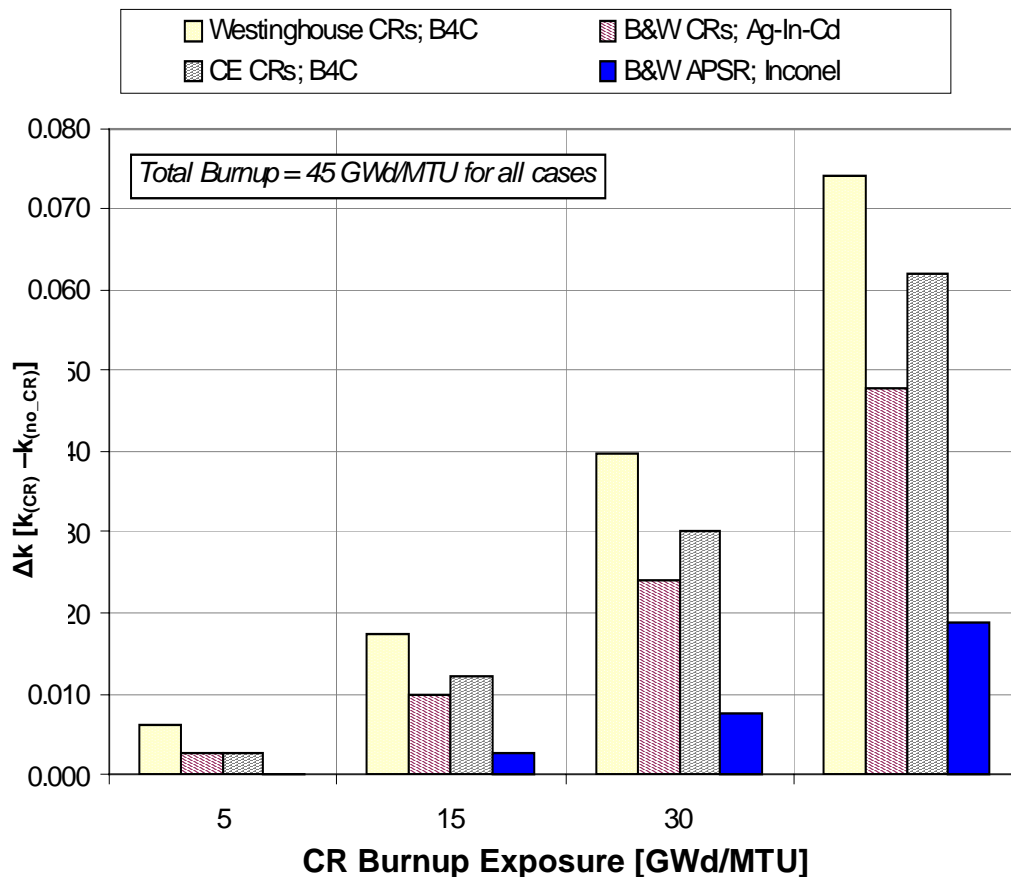


Figure 22 Comparison of Δk values for an infinite assembly array (45 GWd/MTU, 0-year cooling time) with various CR exposures. The results correspond to fuel with 4.0 wt % ^{235}U initial enrichment.

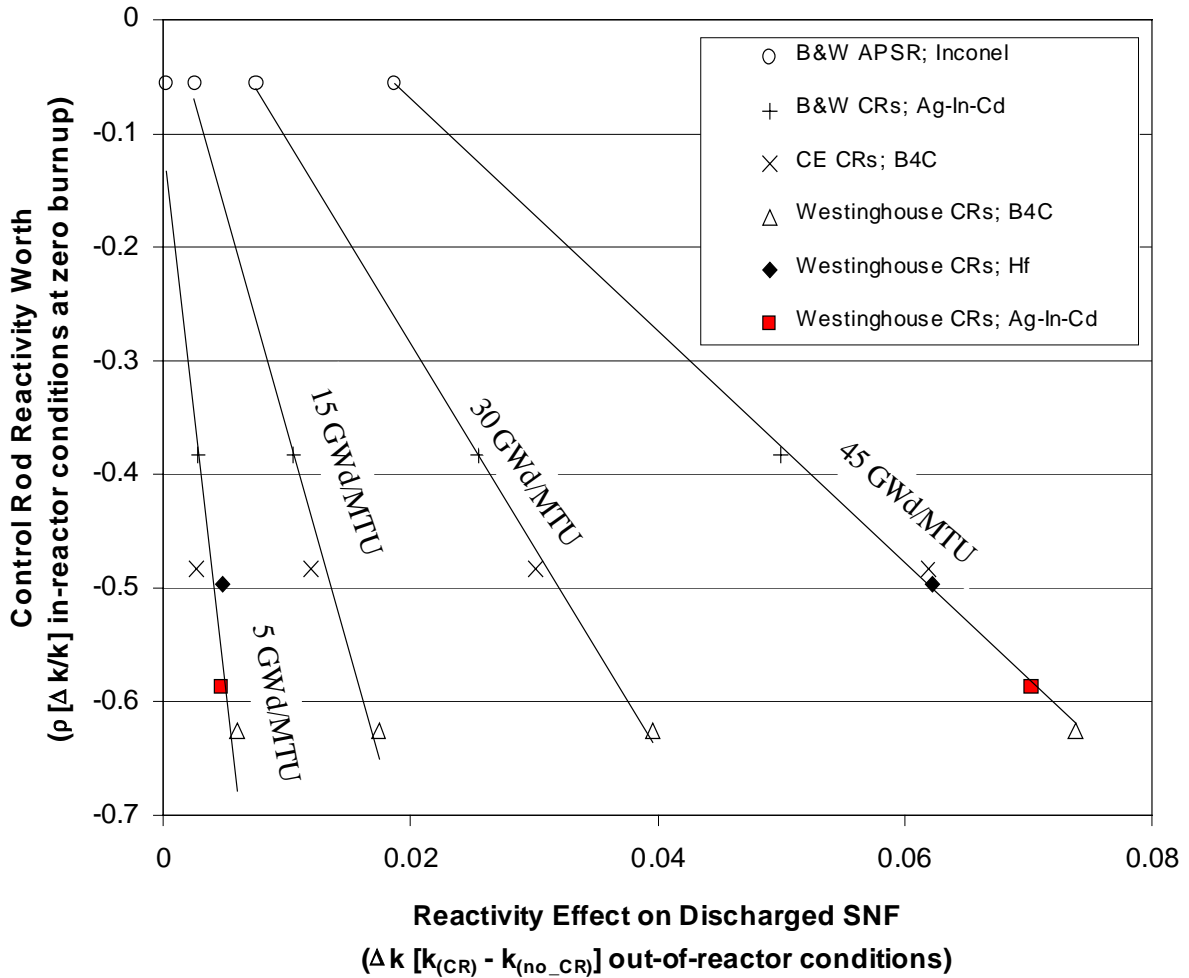


Figure 23 Relationship between the effect of CR exposure on discharge reactivity (in terms of Δk) and CR initial reactivity worth (in terms of $\Delta k/k$) for each of the CR and APSR designs considered. The results correspond to fuel with 45 GWd/MTU burnup and 4.0 wt % ^{235}U initial enrichment that have experienced different CR exposure durations. CR exposure durations are continuous, beginning at zero burnup and continuing until the specified burnup exposure (e.g., 5 GWd/MTU exposure occurs from 0–5 GWd/MTU.)

3.3 THREE-DIMENSIONAL ANALYSES

Although the 2-D analyses presented in the previous section correspond to full axial CR insertion, CRs are not fully inserted during power operations. As stated earlier, the goal of the 2-D analysis was to establish trends and upper bounds; the results overestimate the reactivity effect of CR exposure on actual discharged SNF. The majority of the time, CRs are completely withdrawn from the active fuel region. At other times, the CRs may be inserted into a small upper portion of the active fuel. Any realistic modeling of CR exposure should represent the partial axial insertion, which requires 3-D calculations. Therefore, 3-D calculations are performed and presented in this section to achieve a more accurate and realistic assessment of the effect of CR exposure on the reactivity of discharged SNF.

3.3.1 Code Description

The criticality calculations presented in the following subsections were performed using the KENO V.a module of the SCALE system.¹⁸ KENO V.a is a multigroup Monte Carlo criticality program employed to calculate the neutron multiplication factor, k_{eff} , of a 3-D system. The KENO V.a criticality calculations used the SCALE 238-group cross sections based on ENDF/B-V data. The spent fuel isotopics used in the KENO V.a calculations were calculated using the HELIOS-1.6 code package.¹⁷

3.3.2 Reactivity Behavior with CRs Present for a Rail-Type Cask

The results in Section 3.2 provide understanding of the general behavior of reactivity as a function of burnup when assemblies are exposed to fully-inserted CRs and establish an upper-bound for their impact on the reactivity of discharged SNF. In this section, the effect of CR exposure on SNF loaded in a high-capacity rail-type cask is briefly examined and quantified. First, calculations are performed for conditions in which the CRs are assumed to be fully-inserted during depletion. These results may be compared to the 2-D infinite assembly array results in the previous section to assess the impact of the cask environment on the calculated Δk values. Then, to better approximate realistic CR insertion conditions, calculations are presented for variations in CR exposure in terms of axial insertion and burnup duration.

For this analysis, the generic 32 PWR-assembly Burnup Credit (GBC-32) cask was used. A physical description of the cask is provided in Ref. 19 and a cross-sectional view of the computer model, as prepared by KENO V.a, is shown in Figure 24. The GBC-32 design was developed to provide a reference cask configuration that is representative of typical high-capacity rail casks being considered by industry. The boron loading in the Boral panels in the GBC-32 cask is $0.0225 \text{ g }^{10}\text{B}/\text{cm}^2$.

For the analyses in the previous section, the depletion and criticality calculation were both performed with the HELIOS-1.6 code package and the criticality calculations included all of the nuclides available in the HELIOS-1.6 data library. For the criticality calculations in the following 3-D analyses, the isotopic compositions are calculated by HELIOS, and subsequently extracted for use in KENO V.a input. Therefore, it is necessary to identify the isotopes considered. The use of a subset of possible actinides in burnup credit calculations is referred to as “actinide-only” burnup credit. The nuclides used here for actinide-only calculations are consistent with those specified in a DOE Topical Report on Burnup Credit,⁵ with the exception that ^{236}U and ^{237}Np are also included. While not commonly defined, the use of a subset of possible actinides and fission products will be referred to herein as “actinide + fission product” burnup credit. The nuclides used here for actinide + fission product calculations are consistent with those identified in Table 2 of Ref. 20 as being the most important for burnup credit criticality calculations. Table 10 lists the nuclides included for the two classifications of burnup credit. These “classes” of burnup credit and the nuclides included within each are defined here for the purposes of discussion; other terminology and specific sets of nuclides have been defined and used by others studying burnup credit phenomena.

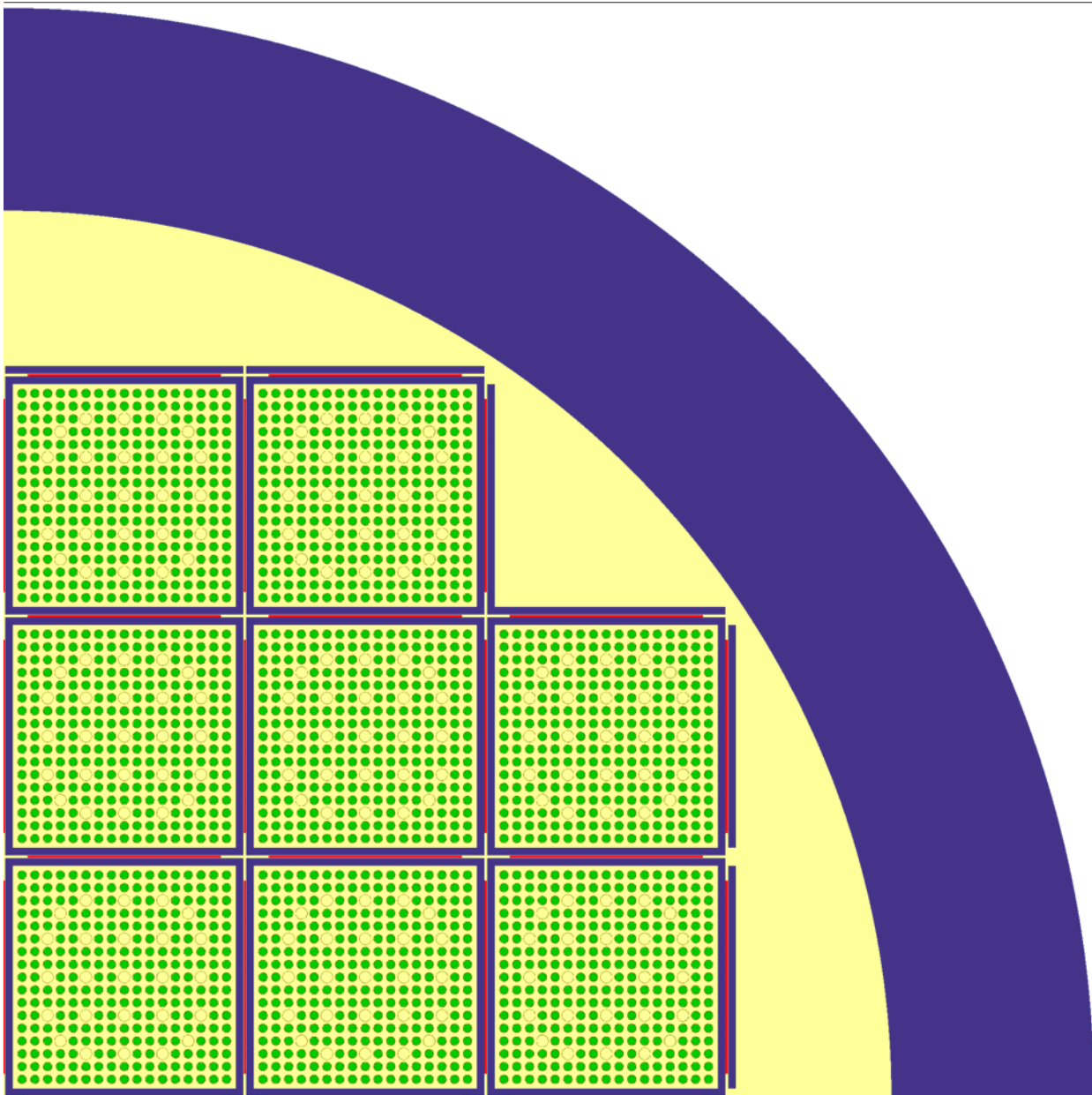


Figure 24 Cross-sectional view of one quarter of the KENO V.a computational model of the GBC-32 cask loaded with Westinghouse 17×17 assemblies

Table 10 Nuclides associated with the various classifications of burnup credit

Actinide-Only Burnup Credit Nuclides (12 total)									
²³⁴ U	²³⁵ U	²³⁶ U	²³⁸ U	²³⁸ Pu	²³⁹ Pu	²⁴⁰ Pu	²⁴¹ Pu	²⁴² Pu	²³⁷ Np
²⁴¹ Am	O								
Actinide + Fission Product Burnup Credit Nuclides (29 total)									
²³⁴ U	²³⁵ U	²³⁶ U	²³⁸ U	²³⁸ Pu	²³⁹ Pu	²⁴⁰ Pu	²⁴¹ Pu	²⁴² Pu	²⁴¹ Am
²⁴³ Am	²³⁷ Np	⁹⁵ Mo	⁹⁹ Tc	¹⁰¹ Ru	¹⁰³ Rh	¹⁰⁹ Ag	¹³³ Cs	¹⁴⁷ Sm	¹⁴⁹ Sm
¹⁵⁰ Sm	¹⁵¹ Sm	¹⁵² Sm	¹⁴³ Nd	¹⁴⁵ Nd	¹⁵¹ Eu	¹⁵³ Eu	¹⁵⁵ Gd	O	
† Oxygen is neither an actinide nor a fission product, but is included in this list because it is included in the calculations.									

3.3.2.1 Full-Axial Insertion Analyses

The k_{eff} values for actinide-only and actinide + fission product burnup credit in the GBC-32 cask loaded with Westinghouse 17×17 OFA assemblies, assuming uniform axial burnup, for various CR exposures are listed in Tables 11 and 12, respectively. The results correspond to fuel with 4 wt % ²³⁵U initial enrichment that has been exposed to fully-inserted Westinghouse hybrid B₄C CRs while accumulating a burnup of 45 GWd/MTU. The Δk values based on actinides only are essentially the same as those calculated based on actinides + fission products. Note that the Δk values in the cask environment are shown to be somewhat larger than those predicted by the infinite assembly array calculations presented in the previous section, and the amount by which they are larger increases with increasing CR exposure. These differences were also observed with HELIOS criticality calculations simulating an infinite array of cask storage cells and are attributed to the fact that the neutron absorber in the cask environment (¹⁰B in the Boral panels) competes for neutrons with the absorbers in the SNF composition, which influences their reactivity worth. The results in Tables 11 and 12 correspond to calculations in which the CRs are assumed to contain B₄C over the full axial length. In contrast, Tables 13 and 14 present results for calculations in which the actual axial variation in absorber material (B₄C/Ag-In-Cd) was included. Note that since we are interested in the impact of CR exposure on the reactivity of SNF, these results consider CRs present during depletion only (i.e., CRs are not included in the KENO V.a model).

The k_{eff} values for actinide-only and actinide + fission product burnup credit in the GBC-32 cask loaded with B&W 15×15 fuel assemblies, assuming uniform axial burnup, for various CR exposures are listed in Tables 15 and 16, respectively. The results correspond to fuel with 4 wt % ²³⁵U initial enrichment that has been exposed to fully-inserted B&W Ag-In-Cd CRs while accumulating a burnup of 45 GWd/MTU. Consistent with the results shown for the Westinghouse CRs, the Δk values with and without fission products are essentially the same and are somewhat larger than those predicted by the 2-D assembly array calculations.

Table 11 Value of k_{eff} for various CR exposures for actinide-only burnup credit in the GBC-32 cask. Results correspond to Westinghouse 17×17 fuel with 4 wt % ^{235}U enrichment, 45 GWd/MTU burnup, zero year cooling, and B₄C CRs fully inserted for various burnup durations

CR exposure (GWd/MTU)	KENO V.a k_{eff}	Standard deviation	Δk ($k_{\text{CRs}} - k_{\text{noCRs}}$)
0	0.9110	0.0005	N/A
5	0.9194	0.0005	0.0084
15	0.9315	0.0006	0.0205
30	0.9592	0.0005	0.0482
45	1.0051	0.0006	0.0941

Table 12 Value of k_{eff} for various CR exposures for actinide + fission product burnup credit in the GBC-32 cask. Results correspond to Westinghouse 17×17 fuel with 4 wt % ^{235}U enrichment, 45 GWd/MTU burnup, zero year cooling, and B₄C CRs fully inserted for various burnup durations

CR exposure (GWd/MTU)	KENO V.a k_{eff}	Standard deviation	Δk ($k_{\text{CRs}} - k_{\text{noCRs}}$)
0	0.8345	0.0005	N/A
5	0.8422	0.0005	0.0077
15	0.8557	0.0006	0.0212
30	0.8832	0.0006	0.0487
45	0.9237	0.0005	0.0892

Table 13 Value of k_{eff} for various CR exposures for actinide-only burnup credit in the GBC-32 cask. Results correspond to Westinghouse 17×17 fuel with 4 wt % ^{235}U enrichment, 45 GWd/MTU burnup, zero year cooling, and B_4C (top part, approximately 160 cm)/ Ag-In-Cd (lower part, approximately 102 cm) CRs fully inserted for various burnup durations

CR Exposure (GWd/MTU)	KENO V.a k_{eff}	Standard deviation	Δk ($k_{\text{CRs}} - k_{\text{noCRs}}$)
0	0.9110	0.0005	N/A
5	0.9189	0.0005	0.0079
15	0.9332	0.0005	0.0222
30	0.9609	0.0005	0.0499
45	1.0039	0.0006	0.0929

Table 14 Value of k_{eff} for various CR exposures for actinide + fission product burnup credit in the GBC-32 cask. Results correspond to Westinghouse 17×17 fuel with 4 wt % ^{235}U enrichment, 45 GWd/MTU burnup, zero year cooling, and B_4C (top part, approximately 160 cm)/ Ag-In-Cd (lower part, approximately 102 cm) CRs fully inserted for various burnup durations

CR Exposure (GWd/MTU)	KENO V.a k_{eff}	Standard deviation	Δk ($k_{\text{CRs}} - k_{\text{noCRs}}$)
0	0.8345	0.0005	N/A
5	0.8419	0.0004	0.0074
15	0.8553	0.0004	0.0208
30	0.8828	0.0005	0.0483
45	0.9232	0.0006	0.0887

Table 15 Value of k_{eff} for various CR exposures for actinide-only burnup credit in the GBC-32 cask. Results correspond to B&W 15×15 fuel with 4 wt % ^{235}U enrichment, 45 GWd/MTU burnup, zero year cooling, and Ag-In-Cd CRs fully inserted for various burnup durations

CR Exposure (GWd/MTU)	KENO V.a k_{eff}	Standard deviation	Δk ($k_{CRs} - k_{noCRs}$)
0	0.9371	0.0006	N/A
5	0.9393	0.0005	0.0022
15	0.9497	0.0005	0.0126
30	0.9680	0.0006	0.0309
45	1.0021	0.0005	0.0650

Table 16 Value of k_{eff} for various CR exposures for actinide + fission product burnup credit in the GBC-32 cask. Results correspond to B&W 15×15 fuel with 4 wt % ^{235}U enrichment, 45 GWd/MTU burnup, zero year cooling, and Ag-In-Cd CRs fully inserted for various burnup durations

CR Exposure (GWd/MTU)	KENO V.a k_{eff}	Standard deviation	Δk ($k_{CRs} - k_{noCRs}$)
0	0.8566	0.0006	N/A
5	0.8602	0.0005	0.0036
15	0.8691	0.0006	0.0125
30	0.8880	0.0005	0.0314
45	0.9185	0.0004	0.0619

The k_{eff} values for actinide-only and actinide + fission product burnup credit in the GBC-32 cask loaded with CE 14×14 fuel assemblies, assuming uniform axial burnup, for various CR exposures are listed in Tables 17 and 18, respectively. The results correspond to fuel with 4 wt % ^{235}U initial enrichment that has been exposed to fully-inserted CE B_4C CRs while accumulating a burnup of 45 GWd/MTU. Upon comparing the Δk values of actinide-only versus the Δk values of actinide + fission products it can be seen that the reactivity behavior is essentially the same. When comparing the results of these calculations in the GBC-32 cask to those shown in previous sections for an infinite assembly arrays, it is apparent that the CR effect is marginally larger in the cask configuration.

Table 17 Value of k_{eff} for various CR exposures for actinide-only burnup credit in the GBC-32 cask. Results correspond to CE 14×14 fuel with 4 wt % ^{235}U enrichment, 45 GWd/MTU burnup, zero year cooling, and B₄C CRs fully inserted for various burnup durations

CR Exposure (GWd/MTU)	KENO V.a k_{eff}	Standard deviation	Δk ($k_{\text{CRs}} - k_{\text{noCRs}}$)
0	0.8809	0.0005	N/A
5	0.8826	0.0005	0.0017
15	0.8936	0.0005	0.0127
30	0.9145	0.0005	0.0336
45	0.9491	0.0006	0.0682

Table 18 Value of k_{eff} for various CR exposures for actinide + fission product burnup credit in the GBC-32 cask. Results correspond to CE 14×14 fuel with 4 wt % ^{235}U enrichment, 45 GWd/MTU burnup, zero year cooling, and B₄C CRs fully inserted for various burnup durations

CR Exposure (GWd/MTU)	KENO V.a k_{eff}	Standard deviation	Δk ($k_{\text{CRs}} - k_{\text{noCRs}}$)
0	0.8053	0.0005	N/A
5	0.8090	0.0004	0.0037
15	0.8191	0.0005	0.0138
30	0.8390	0.0005	0.0337
45	0.8736	0.0005	0.0683

3.3.2.2 Partial-Axial Insertion Analyses

In this section, 3-D calculations are performed with the GBC-32 cask to establish the reactivity effect of CR exposure as a function of axial insertion. For each CR design considered, a series of calculations were performed to determine the effect of various axial depths of CR insertion. The criticality models included isotopics from depletion calculations with CRs present (in the axial region representing the CR insertion) and isotopics from depletion calculations without CRs present (in the remaining axial region). Figure 25 provides an illustration of the partial CR insertion and the criticality model.

The first series of calculations was performed with the Westinghouse 17×17 OFA assembly and the hybrid $B_4C/Ag-In-Cd$ CRs. The Δk values for actinide-only and actinide + fission product burnup credit in the GBC-32 cask as a function of axial CR insertion depth are shown in Figure 26. In accordance with the actual design, the axial variation in CR absorber material [B_4C absorber in the top part of the CR (approximately 260 cm) and $Ag-In-Cd$ absorber in the bottom part (approximately 102 cm)] was modeled. The results correspond to fuel with 4 wt % ^{235}U initial enrichment that has been exposed to Westinghouse hybrid $B_4C/Ag-In-Cd$ rods for the first 5, 15, and 45 GWd/MTU while accumulating a total burnup of 45 GWd/MTU. The KENO V.a models include the axial variation in the depletion isotopics due to CR exposure, but assume uniform axial burnup. The results show that even for significant burnup exposures, minor axial CR insertions (e.g., <20 cm) result in an insignificant effect on the k_{eff} of the cask. Note also that for the cases with CRs, all assemblies in the 32-assembly GBC-32 cask are assumed to have the same CR exposure, which is conservative considering the number of assemblies per core that are positioned under CR clusters.

The calculations were repeated for the B&W 15×15 fuel assemblies employing $Ag-In-Cd$ CRs. The Δk values for actinide-only and actinide + fission product burnup credit in the GBC-32 cask as a function of axial CR insertion depth are shown in Figure 27. The results correspond to spent fuel with 4 wt % ^{235}U initial enrichment that has been exposed to B&W $Ag-In-Cd$ CRs for the first 5, 15, and 45 GWd/MTU while accumulating a total burnup of 45 GWd/MTU. Consistent with the results for the Westinghouse hybrid CRs, the effect of minor axial CR insertions is shown to be very small. Further, the effect is shown to be even smaller for the B&W $Ag-In-Cd$ CRs than what is seen for the Westinghouse hybrid CRs.

Finally, the calculations were repeated for the CE 14×14 fuel assemblies employing $B_4C/Ag-In-Cd$ CRs. Consistent with the actual design, the axial variation in the CR absorber material [B_4C absorber in the top part of the CR (approximately 315 cm) and $Ag-In-Cd$ absorber in the bottom part (approximately 20 cm)] was modeled. The Δk values for actinide-only and actinide + fission product burnup credit in the GBC-32 cask as a function of axial CR insertion depth are shown in Figure 28. The results correspond to spent fuel with 4 wt % ^{235}U initial enrichment that has been exposed to CE B_4C CRs for the first 5, 15, and 45 GWd/MTU while accumulating a total burnup of 45 GWd/MTU. Consistent with the results for the Westinghouse hybrid CRs, the effect of minor axial CR insertions is shown to be insignificant.

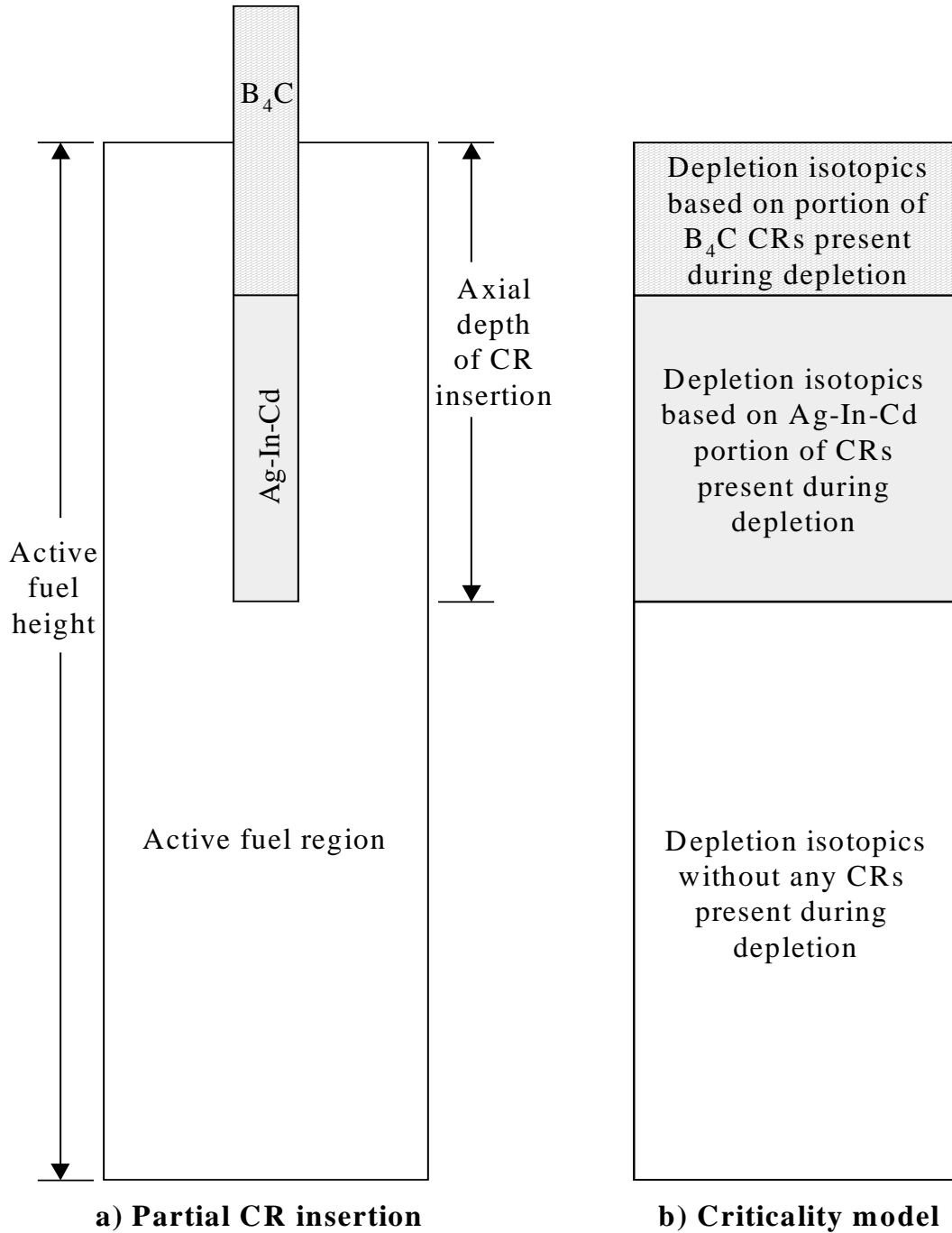


Figure 25 Illustration of (a) partially inserted control rods and (b) a cross section of the criticality model

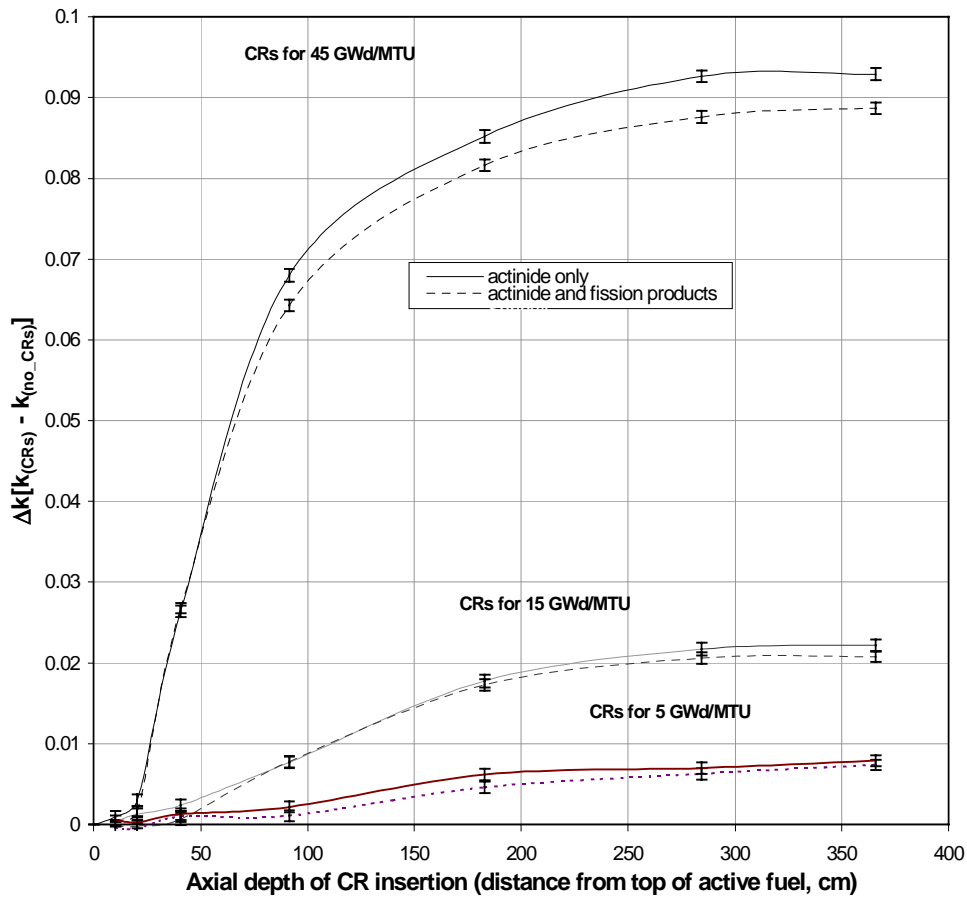


Figure 26 Δk as a function of axial depth of CR insertion for the GBC-32 cask. Results correspond to 4 wt % ^{235}U enriched Westinghouse 17×17 fuel and $\text{B}_4\text{C}/\text{Ag-In-Cd}$ CRs.

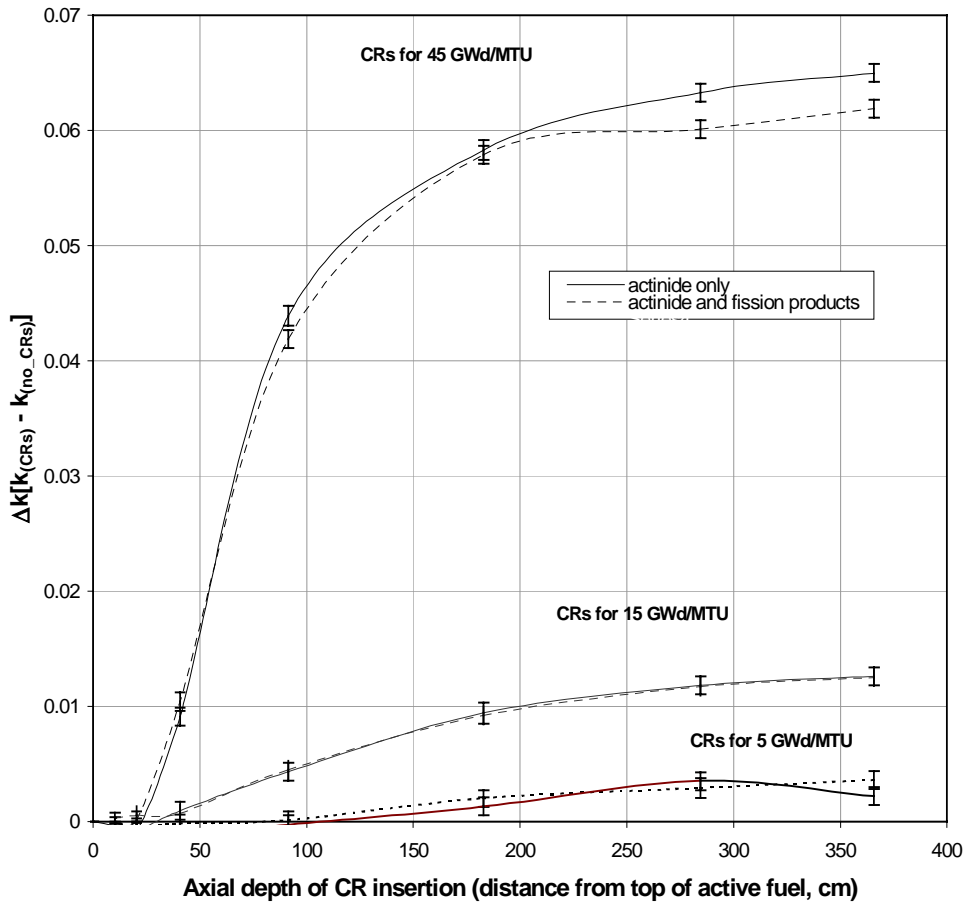


Figure 27 Δk as a function of axial depth of CR insertion for the GBC-32 cask. Results correspond to 4 wt % ^{235}U enriched B&W 15×15 fuel and Ag-In-Cd CRs.

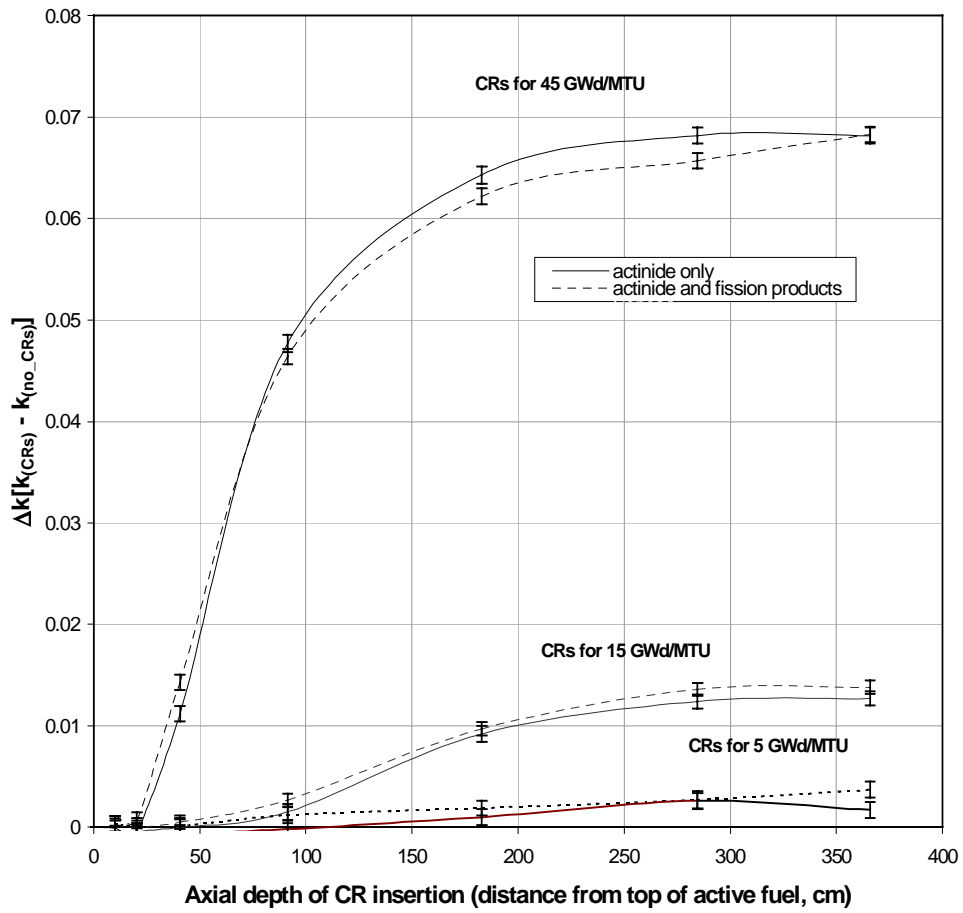


Figure 28 Δk as a function of axial depth of CR insertion for the GBC-32. Results correspond to 4 wt % ^{235}U enriched CE 14×14 fuel and B_4C CRs.

4 DISCUSSION AND IMPLICATIONS

Because of spectral hardening, an assembly exposed to CRs can have a higher reactivity for a given burnup than an assembly that has not been exposed to CRs. While it is known that CRs are typically fully withdrawn from the active fuel region during operation, exceptions to this practice exist. Consequently, a wide range of CR exposure conditions and initial fuel enrichments were studied in order to establish a better understanding of their effect. The first part of Section 3 (2-D analyses) provides understanding of the general behavior of reactivity as a function of burnup when assemblies are exposed to CRs and presents some worst-case CR exposure scenarios. The reactivity effect of CRs was shown to increase with increasing burnup and decreasing initial fuel enrichment. Control rod exposure is shown to have a larger effect on discharge reactivity when it occurs later in the assembly burnup. For variations in CR design, there exists a direct relationship between the reactivity worth of the CRs and their effect on discharge reactivity – higher reactivity worth CRs result in larger effect on discharge reactivity. For the various CR designs considered, maximum reactivity effects are shown to be between 3 and 10% Δk , depending on initial fuel enrichment, when maximum worst-case CR exposure was assumed for a discharge burnup of 45 GWd/MTU.

Unlike the other CR designs, APSRs are commonly utilized in the core for longer periods of time during operation. The reactivity effect of gray APSRs was found to be much less than that of the other CR designs (for a given burnup exposure). The maximum reactivity increases of the gray APSR cases considered are shown to be between 1 and 3% Δk , depending on initial enrichment, when maximum worst-case exposure was assumed for a discharge burnup of 45 GWd/MTU. These 2-D calculations simulated worst-case, unrealistic conditions (i.e., full-axial CR insertion for long periods of burnup), but were effective for gaining a better understanding of the impact of CR and APSR exposure and establishing an upper bound on the reactivity effect.

The second part of Section 3 (3-D analyses) presents the effect of CRs within a high-capacity rail-type cask. KENO V.a calculations were performed to establish the reactivity effect of CR exposure as a function of axial insertion. For each CR design considered, a series of calculations were performed to determine the effect of partially inserted CRs for various burnup exposures. The results show that even for significant burnup exposures, minor axial CR insertions (e.g., < 20 cm) result in an insignificant effect on the k_{eff} of the cask. This conclusion is considered to be important and relevant to current U.S. PWR operations. In addition, the analyses quantify the reactivity effect of intermediate and significant CR insertions, which have relevance to early domestic PWR operations and operations in French PWRs.

Although it is assumed that U.S. PWRs do not currently use CRs to a significant extent (i.e., CRs are not inserted deeper than the top ~20 cm of the active fuel and CRs are not inserted for extended periods of time), this assumption has not been rigorously confirmed. Finally, it is worth noting that operating conditions for French PWRs involve long periods of CR insertion for reactor control, low-power operations and load-following.⁷ Consequently, proposed approaches for burnup credit in France include full CR insertion.⁷

5 RECOMMENDATIONS

The analyses presented in this report provide a technical understanding of the effect of CR exposure on the reactivity of discharged SNF. The analyses demonstrate that the effect increases with increasing CR exposure and decreasing fuel enrichment. Much of the report involves establishing the reactivity effect of CRs with burnup exposure, fuel enrichment, and absorber material to increase understanding. However, and more importantly in terms of practical considerations, 3-D analyses are also described in which the reactivity effect of CRs is assessed as a function of axial CR insertion. These more realistic calculations show that even for significant burnup exposures, minor axial CR insertions (e.g., <20 cm) result in a very small effect on the k_{eff} of a burnup credit cask. Consequently, it is concluded that, based on the assumption that U.S. PWRs do not use CRs to a significant extent (i.e., CRs are not inserted deeper than the top ~20 cm of the active fuel and CRs are not inserted for extended burnups), the effect of CRs on discharge reactivity is relatively small (less than 0.2% Δk). Note that the effect of CR insertion on the axial burnup distribution is not addressed here because it is considered in the selection of the bounding axial profile(s). Unfortunately, the conclusion is dependent on CR operating conditions, which are not comprehensively known to the authors of this report. Therefore, it is recommended that future efforts focus on achieving a greater understanding of CR usage in U.S. PWRs. A detailed understanding of CR usage, coupled with the results presented in this report, will enable the development of a sound technical basis for addressing CR exposure in PWR burnup credit criticality safety evaluations.

6 REFERENCES

1. Spent Fuel Project Office Interim Staff Guidance – 8, Rev. 1 – Limited Burnup Credit, U.S. Nuclear Regulatory Commission, July 30, 1999.
2. D. E. Carlson, C. J. Withee and C. V. Parks, “Spent Fuel Burnup Credit in Casks: An NRC Perspective,” *U.S. Nuclear Regulatory Commission, Proceedings of the Twenty-Seventh Water Reactor Safety Information Meeting*, October 25–27, 1999, Bethesda, Maryland, NUREG/CP-0169, pp. 419–436 (March 2000).
3. J. C. Wagner and C.V. Parks, “Impact of Burnable Poison Rods on PWR Burnup Credit Criticality Safety Analyses,” *Trans. Am. Nucl. Soc.*, **83**, 130–134 (Nov. 2000).
4. C. E. Sanders and J. C. Wagner, *Study of the Effect of Integral Burnable Absorbers for PWR Burnup Credit*, ORNL/TM-2000/321, Oak Ridge National Laboratory (2002).
5. Topical Report on Actinide-Only Burnup Credit for PWR Spent Nuclear Fuel Packages, DOE/RW-0472, Rev. 2, U.S. Department of Energy, Office of Civilian Radioactive Waste Management, September 1998, Washington, DC.
6. J. C. Wagner, "Addressing the Axial Burnup Distribution in PWR Burnup Credit Criticality Safety," 35218.pdf in *Proc. of 2001 ANS Embedded Topical Meeting on Practical Implementation of Nuclear Criticality Safety*, November 11–15, 2001, Reno, NV.
7. M. Maillot, E. Guillou, D. Biron, and S. Janski, "Search for an Envelope Axial Burnup Profile for Use in PWR Criticality Studies with Burnup Credit," in *Proc. ICNC'99, Sixth International Conference on Nuclear Criticality Safety*, September 20–24, 1999, Versailles, France.
8. *CRWMS M&O 1998 Summary Report of Commercial Reactor Criticality Data for Sequoyah Unit 2*, B00000000-01717-5705-00064 Rev. 01, Las Vegas, Nevada: CRWMS M&O. MOL.19980716.0015.
9. M. D. DeHart, *SCALE-4 Analysis of Pressurized Water Reactor Critical Configurations: Volume 1 – Three Mile Island Unit 1 Cycle 5*, ORNL/TM-12294, Vol. 3, Martin Marietta Energy Systems, Inc., Oak Ridge National Laboratory, March 1995.
10. Characteristics of Potential Repository Wastes, DOE/RW-0184-R1, Volume 1, July 1992.
11. Summary Report of Commercial Reactor Criticality Data for Crystal River Unit 3. Document Identifier No.: B00000000-01717-5705-00060 REV 01. April 16, 1998.
12. Calvert Cliffs Nuclear Power Plant UFSAR, Rev. 26 Constellation Nuclear.
13. Hybrid B₄C Absorber Control Rod Evaluation Report. Edited by J. Skaritka. October 1977.
14. Summary Report of Commercial Reactor Criticality Data for Three Mile Island Unit 1. Document Identifier No.: B00000000-01717-5705-00069 REV 00. April 10, 1998.
15. Summary Report of Commercial Reactor Criticality Data for McGuire Unit 1. Document Identifier No.: B00000000-01717-5705-00063 REV 01. April 13, 1998.
16. Summary Report of Commercial Reactor Criticality Data for Sequoyah Unit 2. Document Identifier No.: B00000000-01717-5705-00064 REV 01. April 14, 1998.

17. J. J. Casal, R. J. J. Stamm'ler, E. A. Villarino, and A. A. Ferri, "HELIOS: Geometric capabilities of a new fuel-assembly program," Vol. 2, p. 10.2.1 113, *Intl Topical Meeting on Advances in Mathematics, Computations, and Reactor Physics*, April 28–May 2, 1991, Pittsburgh, Pennsylvania.
18. *SCALE: A Modular Code System for Performing Standardized Computer Analyses for Licensing Evaluation*, NUREG/CR-0200, Rev. 6 (ORNL/NUREG/CSD-2/R6), Vols. I, II, and III, May 2000. Available from Radiation Safety Information Computational Center at Oak Ridge National Laboratory as CCC-545.
19. J. C. Wagner, *Computational Benchmark for Estimation of Reactivity Margin from Fission Products and Minor Actinides in PWR Burnup Credit*, NUREG/CR-6747 (ORNL/TM-2000/306), U.S. Nuclear Regulatory Commission, Oak Ridge National Laboratory, September 2001.
20. C. V. Parks, M. D. DeHart and J. C. Wagner, *Review and Prioritization of Technical Issues Related to Burnup Credit for LWR Fuel*, NUREG/CR-6665 (ORNL/TM-1999/303), U.S. Nuclear Regulatory Commission, Oak Ridge National Laboratory, February 2000.

INTERNAL DISTRIBUTION

1. S. M. Bowman, 6011, MS-6370
2. B. L. Broadhead, 6011, MS-6370
3. W. C. Carter, 6011, MS-6370
4. M. D. DeHart, 6011, MS-6370
5. M. E. Dunn, 6011, MS-6370
6. K. R. Elam, 6011, MS-6370
7. R. J. Ellis, 6025, MS-6363
8. M. B. Emmett, 6011, MS-6370
9. I. C. Gauld, 6011, MS-6370
10. J. C. Gehin, 6025, MS-6363
11. S. Goluoglu, 6011, MS-6370
12. J. N. Herndon, 7601, MS-6305
13. D. F. Hollenbach, 6011, MS-6370
14. C. M. Hopper, 6011, MS
15. D. T. Ingersol, 6025, MS-6362
16. B. L. Kirk, 6025, MS-6435
17. S. B. Ludwig, NTRC, MS
18. G. E. Michaels, 4500N, MS-6210
19. C. I. Moser, 4500N, MS-6199
20. B. D. Murphy, 6011, MS-6370
21. C. V. Parks, 6011, MS-6370
22. L. M. Petrie, 6011, MS-6370
23. R. T. Primm III, 6025, MS-6363
24. B. T. Rearden, 6011, MS-6370
25. J.-P. Renier, 6025, MS-6363
26. C. E. Sanders, 6011, MS-6370
27. J. G. Simpson, 4500N, MS-6210
28. J. C. Wagner, 6011, MS-6370
29. R. M. Westfall, 6011, MS-6370
30. Laboratory Records-RC
4500N, MS-6254
31. Central Research Library
4500N, MS-6191
- 32–50. Return extra ORNL copies to:
W. C. Carter, 6011, MS-6370

EXTERNAL DISTRIBUTION

51. M. L. Anderson, Bechtel SAIC Company, LLC, 1261 Town Center Drive, Las Vegas, NV 89134
52. S. Anton, Holtec International, 555 Lincoln Drive West, Marlton, NJ 08053
53. A. C. Attard, U.S. Nuclear Regulatory Commission, NRR/DSSA/SRXB, MS O10-B1, Washington, DC 20555
54. M. G. Bailey, U.S. Nuclear Regulatory Commission, NMSS, MS T8-A23, Washington, DC 20555-0001
55. A. S. Barto, U.S. Nuclear Regulatory Commission, NMSS/SFPO/TRA, MS O13-D13, Washington, DC 20555-0001
56. C. J. Benson, Bettis Atomic Power Laboratory, P.O. Box 79, West Mifflin, PA 15122
57. G. H. Biding, NUMEC, 17016 Cashell Road, Rockville, MD 20853
58. J. Boshoven, Transnuclear West, Inc., 39300 Civic Center Drive, Suite 280, Fremont, CA 94538
59. M. C. Brady Raap, Battelle, Pacific Northwest National Laboratory, P.O. Box 999 / MS K8-34, Richland, WA 99352

60. R. J. Cacciapouti, Duke Engineering and Services, 400 Donald Lynch Boulevard, Marlborough, MA 01752
61. D. E. Carlson, U.S. Nuclear Regulatory Commission, RES/DSARE/REAHFB, MS T10F-13A, Washington, DC 20555-0001
62. J. M. Conde López, Consejo de Seguridad Nuclear, Jefe de Area de Ingeniería Nuclear, Subdirección General de Tecnología Nuclear, Justo Dorado, 11, 28040 Madrid, Spain
63. D. R. Conners, Bettis Atomic Power Laboratory, P.O. Box 79, West Mifflin, PA 15122
64. P. Cousinou, Institut de Protection et de Sûreté Nucleaire, Département de Recherches en Sécurité, CECI B.P. 6 - 92265 Fontenzy-Aux-Roses, Cedex, France
65. T. W. Doering, Bechtel SAIC Company, LLC, 1261 Town Center Drive, Las Vegas, NV 89134
66. E. P. Easton, U.S. Nuclear Regulatory Commission, NMSS/SFPO/TRD, MS T9-F3, Washington, DC 20555-0001
67. F. Eltawila, U.S. Nuclear Regulatory Commission, NRR/DE, MS O9-E2, Washington, DC 20555-0001
68. K. T. Erwin, U.S. Nuclear Regulatory Commission, NMSS/SFPO/TRB, MS O13-D13, Washington, DC 20555-0001
69. A. Feri, Scandpower, Inc., 101 Lakeforest Blvd. Suite 340, Gaithersburg, MD 20877
70. L. R. Foulke, Bechtel Bettis, Inc., Bettis Atomic Power Laboratory, P.O. Box 79, West Mifflin, PA 15122
71. A. S. Giantelli, U.S. Nuclear Regulatory Commission, NMSS/SFPO/TRA, MS O13-D13, Washington, DC 20555-0001
72. R. N. B. Gmal, Gesellschaft für Anlagen-und Reaktorsicherheit (GRS) mbH, Leiter der Gruppe Kritikalität, Forschungsgelände, 85748 Garching b. München
73. P. Grimm, Paul Scherrer Institute, CH-5232 Villigen Psi, Switzerland
74. N. Gulliford, Winfrith Technology Centre, 306/A32, AEA Technology PLC, Winfrith, Dorchester, Dorset DT2 8DH, United Kingdom
75. J. Guttmann, U.S. Nuclear Regulatory Commission, NMSS/SFPO/TRD, MS O13-D13, Washington, DC 20555-0001
76. A. Haghghat, Nuclear and Radiological Engineering Department, 202 Nuclear Sciences Building, University of Florida, P.O. Box 118300, Gainesville, FL 32611-8300
77. S. Hanauer, U.S. Department of Energy, RW-22, Washington, DC 20545
78. G. Harms, Sandia National Laboratory, PO Box 5800, Mail Stop 1143, Albuquerque, NM 87185-1143
79. L. A. Hassler, Framatome ANP, 3315 Old Forest Road, P.O. Box 10935, Lynchburg, VA 24506-0935
80. D. Henderson, Framatome ANP, 3315 Old Forest Road, P.O. Box 10935, Lynchburg, VA 24506-0935
81. M. W. Hodges, U.S. Nuclear Regulatory Commission, NMSS/SFPO/TRD, MS O13-D13, Washington, DC 20555-0001
82. Hae Ryong Hwang, Radiation Safety Analysis Group, KOPEC, 150, Duckjin Dong, Taejon, South Korea 305-600
83. H. Kühl, Wissenschaftlich-Technische Ingenieurberatung GMBH, Karl-Heinz-Beckurts-Strasse 8, 52428 Jülich
84. W. H. Lake, Office of Civilian Radioactive Waste Management, U.S. Department of Energy, RW-46, Washington, DC 20585
85. D. B. Lancaster, Nuclear Consultants.com, 320 South Corl Street, State College, PA 16801

86. C. Lavarenne, Institut de Protection et de Sûreté Nucléaire, Department of Prevention and Studies of Accidents, Criticality Studies Division, CEA - 60-68, avenue de Général Leclerc, B.P. 6 - 92265, Fontenay - Aux - Roses, Cedex, France
- 87-91. R. Y. Lee, U.S. Nuclear Regulatory Commission, RES/DSARE/SMSAB, MS T10-K8, Washington, DC 20555-0001
92. W. J. Lee, NAC International, 655 Engineerig Drive, Norcross, GA 30092
93. M. Mason, Transnuclear, Two Skyline Drive, Hawthorne, NY 10532-2120
94. A. J. Machiels, Electric Power Research Institute, Advanced Nuclear Technology, Energy Conervation Division, 3412 Hillview Ave., Palo Alto, CA 94304-1395
95. L. Markova, Ustav jaderneho vyzkumu Rez, Theoretical Reactor Physics, Nuclear Research Institute, Czech Republic, 25068 REZ
96. Daniel Marloye, Belgonucléaire, Av. Ariane 4, B-1200, Brussels, Belgium
97. J. R. Massari, Constellation Nuclear Services, 2200 Defense Highway, Suite 405, Crofton, MD 21114-2404
98. C. W. Mays, Framatome ANP, 3315 Old Forest Road, P.O. Box 10935, Lynchburg, VA 24506-0935
99. J. N. McKamy, U.S. Department of Energy, Office of Engineering Assistance and Site Interface, EH-34, 19901 Germantown Rd., Germantown, MD 20874
100. N. B. McLeod, JAI Corporation, 4103 Chain Bridge Road, Suite 200, Fairfax, VA 22030
101. D. Mennerdahl, E. Mennerdahl Systems, Starvägen 12, S-183 57 Täby, Sweden
102. R. L. Murray, 8701 Murray Hill Drive, Raleigh, NC 27615
103. J. A. Myers, U. S. Nuclear Regulatory Commission, NMSS/SFPO/TRD, MS O13-D13, Washington, DC 20555-0001
104. K. A. Neimer, Duke Engineering & Services, 400 S. Tyron St., WC26B, P.O. Box 1004, Charlotte, NC 28201-1004
105. P. Noel, Bechtel SAIC Company, LLC, 1261 Town Center Drive, Las Vegas, NV 89134
106. I. Nojiri, Japan Nuclear Cycle Development Institute, Environment and Safety Division, Tokai Works, Muramatsu Tokai-mura, Naka-gun Ibaraki-ken 319-1194, Japan
107. J. C. Neuber, SIEMENS AG, KWU NS-B, Berliner Str. 295-303, D-63067 OFFENBACH AM MAIN, Germany
108. A. Nouri, OECD/NEA Data Bank, Le Seine-Saint Germain, 12 Boulevard des Iles, F-92130 Issy-les-Moulineaux, France
109. Office of the Assistant Manager for Energy Research and Development, Department of Energy Oak Ridge Operations (DOE-ORO), P.O. Box 2008, Oak Ridge, TN 37831
110. H. Okuno, Japan Atomic Energy Research Institute, Department of Fuel Cycle, Safety Research, 2-4 Shirakata-Shirane, 319-1195 Tokai-mura, Naka-Gun, Ibaraki-ken, Japan
111. P. M. O'Leary, Framatome ANP, 3315 Old Forest Road, P.O. Box 10935, Lynchburg, VA 24506-0935
112. J. R. Massari, Constellation Nuclear Services, 2200 Defense Highway, Suite 405, Crofton, MD 21114-2404
113. N. L. Osgood, U.S. Nuclear Regulatory Commission, Office of Nuclear Materials Safety and Safeguards, MS O13-D13, Washington, DC 20555-0001
114. T. Parish, Department of Nuclear Engineering, Texas A & M University, College Station, TX 77843-3313
115. V. A. Perin, U.S. Nuclear Regulatory Commission, NMSS/FCSS/SPB, MS T8-A33, Washington, DC 20555-0001

116. B. Petrovic, Westinghouse Electric Company, Science and Technology Department, 1344 Beulah Road, Pittsburgh, PA 15235
117. J. S. Philbin, Sandia National Laboratory, PO Box 5800, Mail Stop 1143, Albuquerque, NM 87185-1143
118. M. L. Pitts, Framatome ANP, 3315 Old Forest Road, PO Box 10935, Lynchburg, VA 24506-0935
119. M. Rahimi, U.S. Nuclear Regulatory Commission, NMSS/DWM/HLWB, MS T7-F3, Washington, DC 20555-0001
120. E. L. Redmond II, Holtec International, 555 Lincoln Drive West, Marlton, NJ 08053
121. Frederik Reitsma, Reactor Theory, Building 1900, Pelindaba, NECSA, PO Box 582, 0001 PRETORIA, South Africa
122. C. Rombough, CTR Technical Services, Inc., 5619 Misty Crest Dr., Arlington, TX 76017-4147
123. J. E. Rosenthal, U.S. Nuclear Regulatory Commission, RES/DSARE/SMSAB, MS T10-K8, Washington, DC 20555-0001
124. D. Salmon, Bechtel SAIC Company, LLC, 1261 Town Center Drive, Las Vegas, Nevada 89134
125. A. Santamarina, Commissariat A L'Energie Atomique, Nuclear Reactor Division, Reactor Studies Department, Reactor and Cycle Physics Service, CEA/CADARACHE/DRN/DER/SPRC Bat. 230, 13108 Saint-Paul-Lez-Durance, Cedex, France
126. E. Sartori, OECD/NEA Data Bank, Le Seine-Saint Germain, 12 Boulevard des Iles, F-92130 Issy-les-Moulineaux, France
127. J. J. Sapyta, Framatome ANP, 3315 Old Forest Road, P.O. Box 10935, Lynchburg, VA 24506-0935
128. D. Schrire, Hot Cell Laboratory, Studsvik Nuclear, Nyköping 61182, Sweden
129. H. H. Schweer, Bundesamt fuer Strahlenschutz, Willi Brandt Str. 5, D-38226 SALZGITTER, Germany
130. M. Smith, Virginia Power Co., P.O. Box 2666, Richmond, VA 23261
131. N. R. Smith, AEA Technology, A32 Winfrith, Dorchester, Dorset DT2 8DH, United Kingdom
132. Rudi Stamm'ler, Studsvik Scandpower AS, Gasevikveien 2, P O Box 15, NO-2027 Kjeller Norway
133. J. T. Stewart, Department of Environment, Transport, and Re, RMTD, 4/18, GMH, 76 Marsham Street, London SW1P 4DR, United Kingdom
134. T. Suto, Power Reactor and Nuclear Fuel Development Corporation, Technical Service Division, Tokai Reprocessing Plant, Tokai Works, Tokai-Mura, Naka-gun, Ibaraki-ken, Japan
135. H. Taniuchi, Kobe Steel, Ltd., 2-3-1 Shinhama, Arai-Cho, Takasago, 676 Japan
136. D. A. Thomas, Bechtel SAIC Company, LLC, 1261 Town Center Drive, Las Vegas, NV 89134
137. P. R. Thorne, British Nuclear Fuels plc (BNFL), Nuclear and Radiological Safety, R101 Rutherford House, Risley Warrington WA3 6AS, United Kingdom
138. J. R. Thornton, Duke Engineering & Services, 230 S. Tyron St., P.O. Box 1004, Charlotte, NC 28201-1004
139. S. E. Turner, Holtec International, 230 Normandy Circle East, Palm Harbor, FL 34683
140. A. P. Ulses, U.S. Nuclear Regulatory Commission, NRR/DSSA/SRXB, MS O10-B3, Washington, DC 20555-0001
141. M. E. Wangler, U.S. Department of Energy, EH-33.2, Washington, DC 20585-0002
142. M. D. Waters, U.S. Nuclear Regulatory Commission, NMSS/SFPO/SLID, MS O13-D13, Washington, DC 20555-0001

143. A. Wells, 2846 Peachtree Walk, Duluth, GA 30136
144. S. A. Whaley, U.S. Nuclear Regulatory Commission, NMSS/SFPO/TRD, MS O13-D13, Washington, DC 20555-0001
145. B. H. White, U.S. Nuclear Regulatory Commission, NMSS/SFPO/TRD, MS O13-D13, Washington, DC 20555-0001
146. R. Wilson, Rocky Flats Field Office, USDOE, 10808 Highway 93, Golden, CO 80403-8200
147. C. J. Withee, U.S. Nuclear Regulatory Commission, NMSS/SFPO/TRD, MS O13-D13, Washington, DC 20555-0001

NRC FORM 335 (2-89) NRCM 1102 3201, 3202	U.S. NUCLEAR REGULATORY COMMISSION BIBLIOGRAPHIC DATA SHEET <i>(See instructions on the reverse)</i>	1. REPORT NUMBER (Assigned by NRC, Add Vol., Supp., Rev., and Addendum Numbers, if any.) NUREG/CR-6759 ORNL/TM-2001/69	
2. TITLE AND SUBTITLE Parametric Study of the Effect of Control Rods for PWR Burnup Credit		3. DATE REPORT PUBLISHED	
		MONTH February	YEAR 2002
		4. FIN OR GRANT NUMBER W6479	
5. AUTHOR(S) C. E. Sanders and J. C. Wagner	6. TYPE OF REPORT Technical	7. PERIOD COVERED <i>(Inclusive Dates)</i>	
	8. PERFORMING ORGANIZATION — NAME AND ADDRESS <i>(If NRC, provide Division, Office or Region, U.S. Nuclear Regulatory Commission, and mailing address; if contractor, provide name and mailing address.)</i> Oak Ridge National Laboratory Managed by UT-Battelle, LLC Oak Ridge, TN 37831-6370		
9. SPONSORING ORGANIZATION — NAME AND ADDRESS <i>(If NRC, type "Same as above"; if contractor, provide NRC Division, Office or Region, U.S. Regulatory Commission, and mailing address.)</i> Division of Systems Analysis and Regulatory Effectiveness Office of Nuclear Regulatory Research U.S. Nuclear Regulatory Commission Washington, DC 20555-0001			
10. SUPPLEMENTARY NOTES R. Y. Lee, NRC Project Manager			
11. ABSTRACT <i>(200 words or less)</i> <p>The Interim Staff Guidance on burnup credit for pressurized water reactor (PWR) spent nuclear fuel (SNF), issued by the United States Nuclear Regulatory Commission's Spent Fuel Project Office, recommends the use of analyses that provide an "adequate representation of the physics" and notes particular concern with the "need to consider the more reactive actinide compositions of fuels burned with fixed absorbers or with control rods fully or partly inserted." In the absence of readily available information on the extent of control rod (CR) usage in U.S. PWRs and the subsequent reactivity effect of CR exposure on discharged SNF, NRC staff has indicated a need for greater understanding in these areas. In response, this report presents a parametric study of the effect of CR exposure on the reactivity of discharged SNF for various CR designs, including Axial Power Shaping Rods, fuel enrichments, and exposure conditions (i.e., burnup and axial insertion).</p>			
12. KEY WORDS/DESCRIPTORS <i>(List words or phrases that will assist researchers in locating the report.)</i> criticality safety, burnup credit, transportation, dry storage, control rods, axial power shaping rods	13. AVAILABILITY STATEMENT unlimited		
	14. SECURITY CLASSIFICATION <i>(This Page)</i> unclassified		
	<i>(This Report)</i> unclassified		
	15. NUMBER OF PAGES		
16. PRICE			